Title

Measurements of prompt charm production cross-sections in pp collisions at s=5 TeV

Journal

Journal of High Energy Physics, 2017(6)

ISSN

1126-6708

Authors

The LHCb collaboration
Aaij, R
Adeva, B
et al.

Publication Date

2017-06-01

DOI

10.1007/jhep06(2017)147

EUROPEAN ORGANIZATION FOR NUCLEAR RESEARCH (CERN)

CERN-EP-2016-244
LHCb-PAPER-2016-042
May 11, 2017

Measurements of prompt charm production cross-sections in pp collisions at $\sqrt{s} = 5\,\text{TeV}$

The LHCb collaboration[†]

Abstract

Production cross-sections of prompt charm mesons are measured using data from pp collisions at the LHC at a centre-of-mass energy of 5 TeV. The data sample corresponds to an integrated luminosity of $8.60 \pm 0.33\,\text{pb}^{-1}$ collected by the LHCb experiment. The production cross-sections of D^0, D^+, D_s^+, and D^{*+} mesons are measured in bins of charm meson transverse momentum, p_{T}, and rapidity, y. They cover the rapidity range $2.0 < y < 4.5$ and transverse momentum ranges $0 < p_{\text{T}} < 10\,\text{GeV}/c$ for D^0 and D^+ and $1 < p_{\text{T}} < 10\,\text{GeV}/c$ for D_s^+ and D^{*+} mesons. The inclusive cross-sections for the four mesons, including charge-conjugate states, within the range of $1 < p_{\text{T}} < 8\,\text{GeV}/c$ are determined to be

$$\begin{aligned}
\sigma(pp \to D^0 X) &= 1004 \pm 3 \pm 54\,\mu\text{b}, \\
\sigma(pp \to D^+ X) &= 402 \pm 2 \pm 30\,\mu\text{b}, \\
\sigma(pp \to D_s^+ X) &= 170 \pm 4 \pm 16\,\mu\text{b}, \\
\sigma(pp \to D^{*+} X) &= 421 \pm 5 \pm 36\,\mu\text{b},
\end{aligned}$$

where the uncertainties are statistical and systematic, respectively.

Submitted to JHEP

[†]Authors are listed at the end of this paper.

1 Introduction

Measurements of charm production cross-sections in proton-proton collisions are important tests of perturbative quantum chromodynamics [1–4]. Predictions of charm meson cross-sections have been made at next-to-leading order using the generalised mass variable flavour number scheme (GMVFNS) [3, 5–9] and at fixed order with next-to-leading-log resummation (FONLL) [1, 2, 10–13]. These are based on a factorisation approach, where the cross-sections are calculated as a convolution of three terms: the parton distribution functions of the incoming protons; the partonic hard scattering rate, estimated as a perturbative series in the coupling constant of the strong interaction; and a fragmentation function that parametrises the hadronisation of the charm quark into a given type of charm hadron. Predictions are also obtained from Monte Carlo programs implementing NLO perturbative QCD, where the partonic final state is matched to parton shower simulations [1]. The range of rapidity, y, and of the momentum component transverse to the beam axis, $p_{\rm T}$, accessible to the LHCb experiment enables quantum chromodynamics calculations to be tested in a region where the momentum fraction, x, of the initial state partons can reach values below 10^{-4}. In this region the uncertainties on the gluon density function are large, exceeding 30% [1,14], and LHCb measurements can be used to constrain it. This paper presents measurements of charm hadron production cross-sections at a proton-proton centre-of-mass energy of $\sqrt{s} = 5\,\text{TeV}$. Ratios of cross-sections at different $\sqrt{s}$ benefit from cancellations in experimental uncertainties on the measured cross-sections as well as theoretical uncertainties on the predictions [2], allowing for precise comparisons. Measurements of charm production cross-sections in pp collisions at $\sqrt{s} = 5\,\text{TeV}$ also define the reference for the determination of nuclear modification factors in heavy ion collisions at that nucleon-nucleon centre-of-mass energy, recorded in 2015 at the Large Hadron Collider (LHC).

Measurements of charm production cross-sections in hadronic collisions have been performed in different kinematic regions and for various centre-of-mass energies in the TeV range. Measurements by the CDF experiment cover the central rapidity region $|y| < 1$ and transverse momenta, $p_{\rm T}$, between $5.5\,\text{GeV}/c$ and $20\,\text{GeV}/c$ at $\sqrt{s} = 1.96\,\text{TeV}$ in $p\overline{p}$ collisions [15]. At the LHC, charm cross-sections in pp collisions have been measured in the $|y| < 0.5$ region for $p_{\rm T} > 1\,\text{GeV}/c$ at $\sqrt{s} = 2.76\,\text{TeV}$ and for $p_{\rm T} > 0\,\text{GeV}/c$ at $\sqrt{s} = 7\,\text{TeV}$ by the ALICE experiment [16–19], and for pseudorapidity $|\eta| < 2.1$ in the $p_{\rm T}$ region $3.5 < p_{\rm T} < 100\,\text{GeV}/c$ at $\sqrt{s} = 7\,\text{TeV}$ by the ATLAS experiment [20]. The LHCb experiment has recorded the world's largest dataset of charm hadrons to date and this has led to numerous high-precision measurements of their production and decay properties. LHCb measured the cross-sections in the forward region $2.0 < y < 4.5$ for $0 < p_{\rm T} < 8\,\text{GeV}/c$ at $\sqrt{s} = 7\,\text{TeV}$ [21] and for $0 < p_{\rm T} < 15\,\text{GeV}/c$ at $\sqrt{s} = 13\,\text{TeV}$ [22].

Charm mesons produced at the pp collision point, either directly or as decay products of excited charm resonances, are referred to as promptly produced. No attempt is made to distinguish between these two sources. This paper presents measurements of the cross-sections for the prompt production of D^0, D^+, D_s^+, and $D^*(2010)^+$ (henceforth denoted as D^{*+}) mesons, based on data corresponding to an integrated luminosity of $8.60 \pm 0.33\,\text{pb}^{-1}$. Charm mesons produced through the decays of b hadrons are referred to as secondary charm and are considered here as a background process.

The analysis techniques described in this paper are nearly identical to those used in the measurements made at $\sqrt{s} = 13\,\text{TeV}$ [22], allowing for very precise determination of

the ratios between the two results.

Section 2 describes the detector, data acquisition conditions, and the simulation; this is followed by a summary of the data analysis in Sec. 3. The differential cross-section results are given in Sec. 4 while Sec. 5 presents the measurements of integrated cross-sections and of the ratios of the cross-sections measured at $\sqrt{s} = 5\,\text{TeV}$ to those at 13 TeV. The theoretical predictions and their comparison with the results of this paper are discussed in Sec. 6. Section 7 provides a summary.

2 Detector and simulation

The LHCb detector [23, 24] is a single-arm forward spectrometer covering the pseudorapidity range $2 < \eta < 5$, designed for the study of particles containing b or c quarks. The detector includes a high-precision tracking system consisting of a silicon-strip vertex detector surrounding the pp interaction region, a large-area silicon-strip detector located upstream of a dipole magnet with a bending power of about 4 Tm, and three stations of silicon-strip detectors and straw drift tubes placed downstream of the magnet. The tracking system provides a measurement of momentum of charged particles with a relative uncertainty that varies from 0.5% at low momentum to 1.0% at 200 GeV/c. The minimum distance of a track to a primary vertex (PV), the impact parameter (IP), is measured with a resolution of $(15 + 29/p_{\text{T}})\,\mu\text{m}$, where p_{T} is the component of the momentum transverse to the beam, in GeV/c. Different types of charged hadrons are distinguished by information from two ring-imaging Cherenkov detectors. Photons, electrons and hadrons are identified by a calorimeter system consisting of scintillating-pad and preshower detectors, an electromagnetic calorimeter and a hadronic calorimeter. Muons are identified by a system composed of alternating layers of iron and multiwire proportional chambers.

The online event selection is performed by a trigger. This consists of a hardware stage, which, for this analysis, randomly selects a pre-defined fraction of all beam-beam crossings at a rate of 300 kHz, followed by a software stage. In between the hardware and software stages, an alignment and calibration of the detector is performed in near real-time [25] and updated constants are made available for the trigger. The same alignment and calibration information is propagated to the offline reconstruction, ensuring consistent and high-quality particle identification (PID) information between the trigger and offline software. The identical performance of the online and offline reconstruction offers the opportunity to perform physics analyses directly using candidates reconstructed in the trigger [26, 27], which the present analysis exploits. The storage of only the triggered candidates enables a reduction in the event size by an order of magnitude.

In the simulation, pp collisions are generated with Pythia 8.1 [28, 29] using a specific LHCb configuration similar to the one described in Ref. [30]. Decays of hadronic particles are described by EvtGen [31] in which final-state radiation is generated with Photos [32]. The implementation of the interaction of the generated particles with the detector, and its response, uses the Geant4 toolkit [33] as described in Ref. [34].

3 Analysis strategy

The analysis methodology is very similar to that used to measure the prompt production cross-sections at $\sqrt{s} = 13\,\text{TeV}$ [22], of which a summary is given below. The measurement at $\sqrt{s} = 5\,\text{TeV}$ reconstructs the same final states: $D^0 \to K^-\pi^+$, $D^+ \to K^-\pi^+\pi^+$, $D_s^+ \to (K^-K^+)_\phi\pi^+$ and $D^{*+} \to D^0(\to K^-\pi^+)\pi^+$. Throughout this paper, charge conjugation is implied and thus the $D^0 \to K^-\pi^+$ sample contains the sum of the Cabibbo-favoured decays $D^0 \to K^-\pi^+$ and the doubly Cabibbo-suppressed decays $\overline{D}^0 \to K^-\pi^+$. The $D_s^+ \to (K^-K^+)_\phi\pi^+$ sample comprises all reconstructed $D_s^+ \to K^-K^+\pi^+$ decays where the invariant mass of the K^-K^+ pair falls into a $\pm 20\,\text{MeV}/c^2$ window around the nominal $\phi(1020)$ mass, taken to be $1020\,\text{MeV}/c^2$.

The cross-sections are measured in two-dimensional bins of p_T and y of the reconstructed mesons, where p_T and y are measured in the pp centre-of-mass frame with respect to the pp collision axis. The bin widths are 0.5 in y covering a range of $2.0 < y < 4.5$ and $1\,\text{GeV}/c$ in p_T for $0 < p_\text{T} < 10\,\text{GeV}/c$.

3.1 Selection of candidates

Candidates for D^0, D^+ and D_s^+ mesons are formed in events containing at least one reconstructed PV by combining tracks that have been positively identified as kaons or pions by the LHCb PID system. These tracks are required to be above a transverse momentum threshold that depends on the decay mode, and must be consistent with originating from a common vertex. Due to the long lifetimes of the studied charm mesons, this common vertex is required to be significantly displaced from any reconstructed PV and the displacement vector with respect to the closest PV must align with the combined momentum of the tracks. Candidates for D^{*+} mesons are formed by combining a D^0 and a charged pion candidate, requiring that both form a good quality vertex. Applying the selection, 1% of all events have more than one selected candidate, all of which are considered in this analysis.

The efficiencies for the reconstruction and selection of charm meson candidates are obtained for each (p_T, y) bin in a near-identical manner to the $\sqrt{s} = 13\,\text{TeV}$ measurement [22]. All efficiencies are evaluated using the event simulation, except for the efficiencies for identifying kaons and pions and the tracking efficiencies. Kaon and pion identification efficiencies are evaluated using a high purity calibration sample of $D^{*+} \to D^0(\to K^-\pi^+)\pi^+$ decays which have been selected without PID requirements. Only the correct assignment of the kaon and pion hypotheses for the decay products of the D^0 candidates yields the expected shapes in the mass distributions. The numbers of true kaon and pion tracks in the calibration sample are determined from maximum likelihood fits to the D^0 and D^{*+} candidate invariant mass distributions, as described in Section 3.2. The identification efficiency for a true kaon or pion to pass a given PID requirement is computed by performing these fits in bins of track multiplicity and track kinematics before and after the selection. This technique differs slightly from that used in the analysis of the $\sqrt{s} = 13\,\text{TeV}$ data, where a single maximum likelihood fit was performed on the calibration sample integrated across all bins, and the per-bin kaon and pion yields were computed by summing sWeights [35]. The change leads to a stable solution for sparsely populated bins and is introduced due to the substantially smaller size of the calibration sample compared to the $\sqrt{s} = 13\,\text{TeV}$ measurement. Tracking efficiencies in the simulation are corrected with a

Table 1: Prompt signal yields in the fully selected dataset, summed over all $(p_{\rm T}, y)$ bins in which a measurement is made. Only statistical uncertainties are given.

Hadron	Prompt signal yield
D^0	$(34.4 \pm 0.7) \times 10^4$
D^+	$(27.6 \pm 0.6) \times 10^4$
D_s^+	$(13.2 \pm 0.1) \times 10^3$
D^{*+}	$(39.0 \pm 0.2) \times 10^3$

factor derived from data as described in Ref. [36] with typical values in the range of 0.97 to 1.02.

3.2 Determination of signal yields

The data contain a mixture of prompt signal decays, secondary charm mesons produced in decays of b hadrons, and combinatorial background. While combinatorial background can be distinguished from signal decays in the invariant mass distribution of charm meson candidates, both prompt signal decays and secondary charm mesons have the same mass shape. However, secondary charm mesons will, on average, have a greater IP with respect to the closest PV than prompt signal, and this is exploited by using the spectrum of $\ln(\chi^2_{\rm IP})$ of the charm meson candidates, where $\chi^2_{\rm IP}$ is defined as the difference in χ^2 of the PV fit, performed with and without the particle under consideration.

The prompt signal yield in each $(p_{\rm T}, y)$ bin is obtained from a fit to the $\ln(\chi^2_{\rm IP})$ distribution of the charm meson within a $20\,{\rm MeV}/c^2$ window around the known mass [37] of the D^0, D^+, or D_s^+ meson, corresponding to approximately 2.5 times the mass resolution. For the D^{*+} measurements, an additional signal window around the nominal $\Delta m = m(D^{*+}) - m(D^0)$ value of $145.43\,{\rm MeV}/c^2$ [37] is used, and the fit is made to the $\ln(\chi^2_{\rm IP})$ distribution of the D^0 meson. Candidates outside the signal region are used to construct templates for the combinatorial background shape in the $\ln(\chi^2_{\rm IP})$ distributions. For the D^0, D^+, and D_s^+ measurements, a fit to the invariant mass distributions is used to constrain the number of combinatorial background candidates in the $\ln(\chi^2_{\rm IP})$ fit. A fit to the Δm distribution is used for the D^{*+} measurements. The fits to the invariant mass, Δm, and $\ln(\chi^2_{\rm IP})$ distributions are performed as extended binned maximum likelihood fits, performed simultaneously across all $(p_{\rm T}, y)$ bins. The fit model definitions, and the choice of model parameters that are shared across $(p_{\rm T}, y)$ bins, are identical to those used in the $\sqrt{s} = 13\,{\rm TeV}$ measurement [22].

The sums of the fits over all $(p_{\rm T}, y)$ bins are given in Figs. 1–4. The fits generally describe the data well. Inaccuracies in the description of the data by the fit model are found to have only a small effect on the estimated prompt signal yield and are taken into account as systematic uncertainties. The sums of the prompt signal yields, as determined by the fits, are given in Table 1.

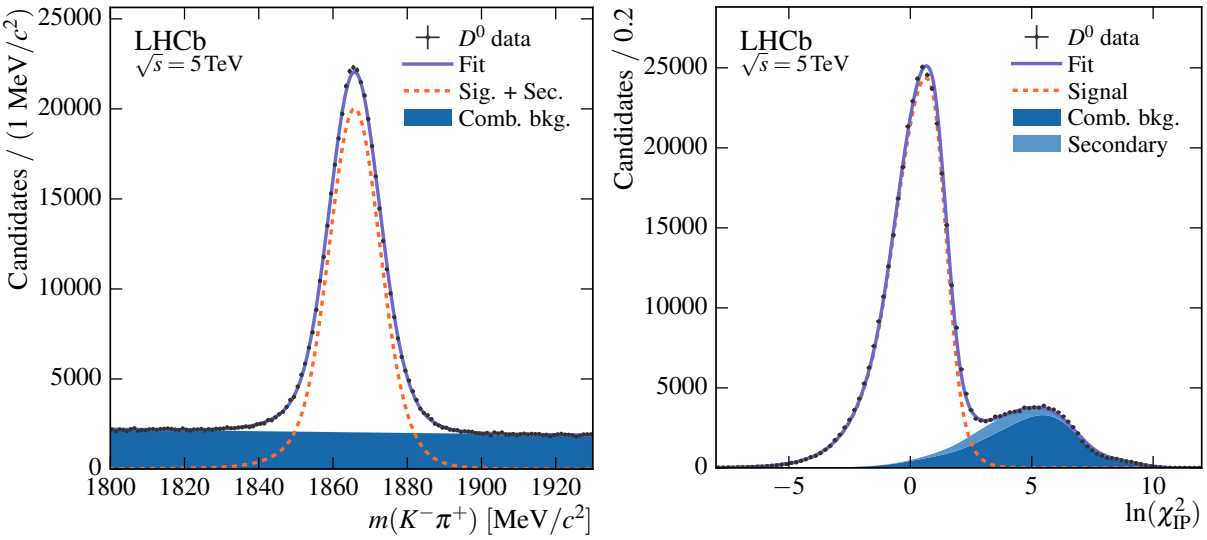

Figure 1: Distributions for selected $D^0 \to K^-\pi^+$ candidates: (left) $K^-\pi^+$ invariant mass and (right) $\ln\left(\chi^2_{\text{IP}}\right)$ for a mass window of $\pm 20\,\text{MeV}/c^2$ around the nominal D^0 mass. The sum of the simultaneous likelihood fits in each (p_{T}, y) bin is shown, with components as indicated in the legends.

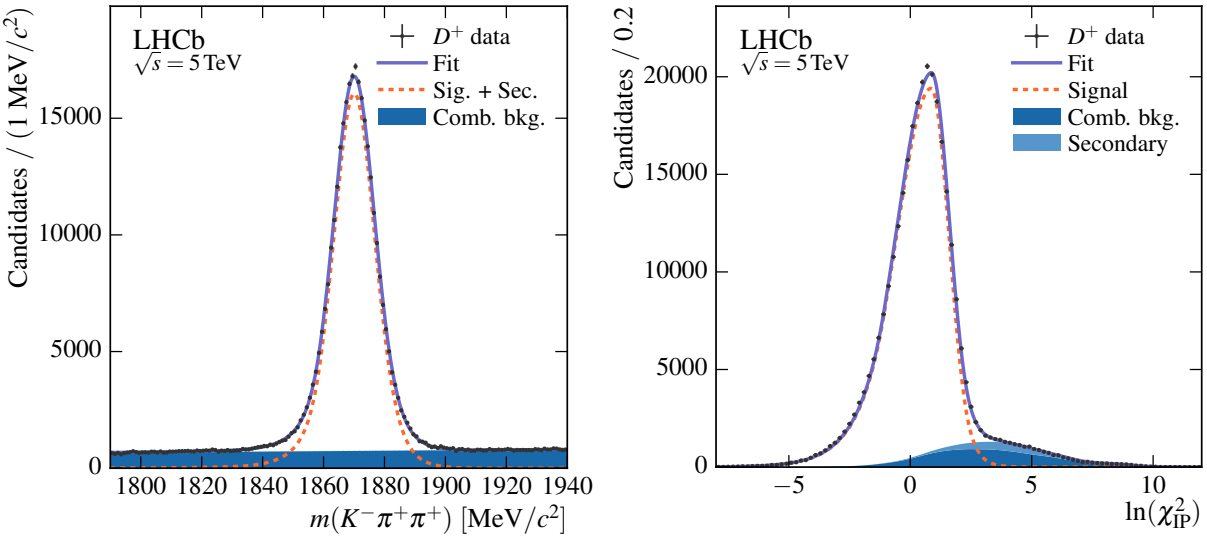

Figure 2: Distributions for selected $D^+ \to K^-\pi^+\pi^+$ candidates: (left) $K^-\pi^+\pi^+$ invariant mass and (right) $\ln\left(\chi^2_{\text{IP}}\right)$ for a mass window of $\pm 20\,\text{MeV}/c^2$ around the nominal D^+ mass. The sum of the simultaneous likelihood fits in each (p_{T}, y) bin is shown, with components as indicated in the legends.

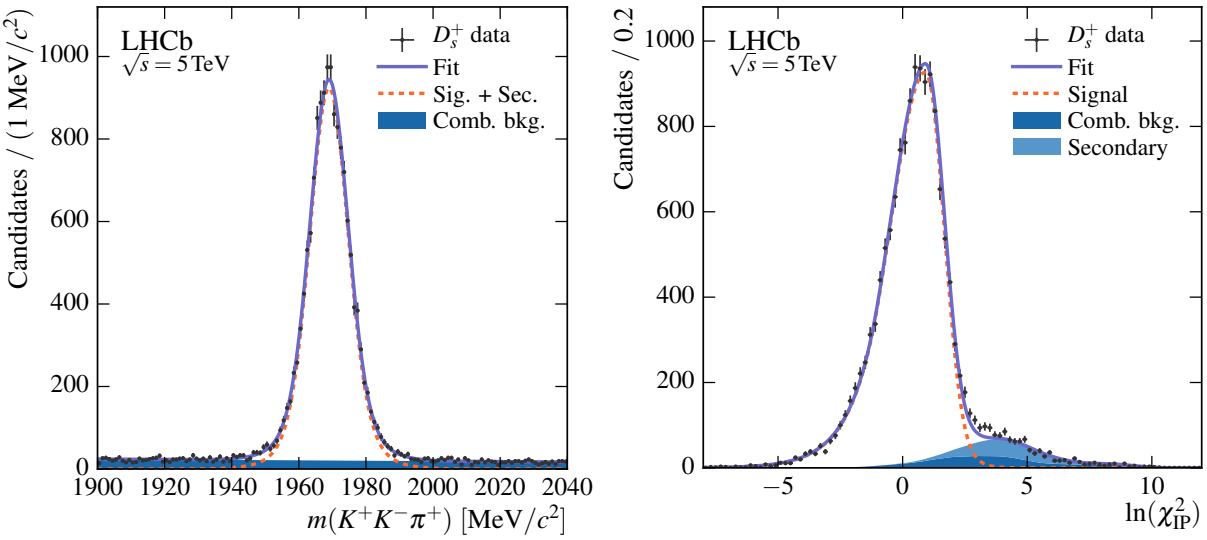

Figure 3: Distributions for selected $D_s^+ \to (K^-K^+)_\phi\pi^+$ candidates: (left) $K^+K^-\pi^+$ invariant mass and (right) $\ln\left(\chi^2_{\text{IP}}\right)$ for a mass window of $\pm 20\,\text{MeV}/c^2$ around the nominal D_s^+ mass. The sum of the simultaneous likelihood fits in each (p_{T}, y) bin is shown, with components as indicated in the legends.

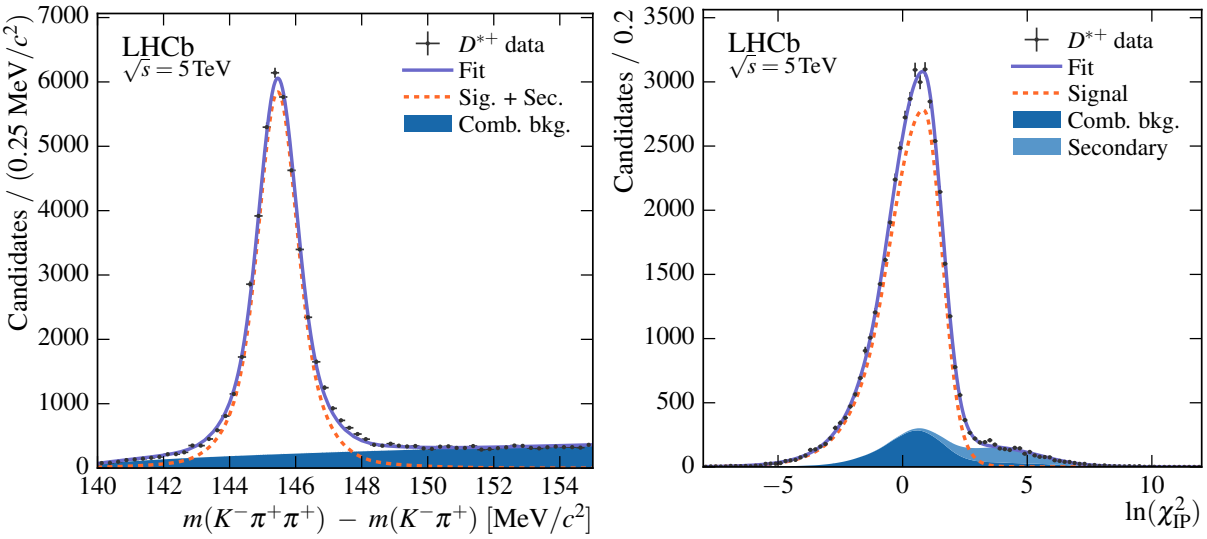

Figure 4: Distributions for selected $D^{*+} \to D^0\pi^+$ candidates, with $D^0 \to K^-\pi^+$: (left) $\Delta m = m(D^{*+}) - m(D^0)$ for a mass window of $\pm 20\,\text{MeV}/c^2$ around the nominal D^0 mass and (right) $\ln\left(\chi^2_{\text{IP}}\right)$ of the D^0 with an additional mass window of $\pm 3\,\text{MeV}/c^2$ around the nominal D^{*+} - D^0 mass difference. The sum of the simultaneous likelihood fits in each (p_{T}, y) bin is shown, with components as indicated in the legends.

4 Cross-section measurements

In each $(p_{\rm T}, y)$ bin i, the bin averaged differential cross-section for producing the charm meson D is calculated from the relation

$$\frac{{\rm d}^2\sigma_i(D)}{{\rm d}p_{\rm T}\,{\rm d}y} = \frac{1}{\Delta p_{\rm T}\Delta y}\cdot\frac{N_i(D\to f+{\rm c.c.})}{\varepsilon_{i,{\rm tot}}(D\to f)\mathcal{B}(D\to f)\,\kappa\,\mathcal{L}_{\rm int}}, \tag{1}$$

where $\Delta p_{\rm T}$ and Δy are the widths in $p_{\rm T}$ and y of bin i, $N_i(D\to f+{\rm c.c.})$ is the measured yield of prompt D decays to the final state f in bin i from the $\ln(\chi^2_{\rm IP})$ fit including the charge-conjugate decay, and $\varepsilon_{i,{\rm tot}}(D\to f)$ is the total efficiency for observing the signal decay in bin i. The total integrated luminosity collected, $\mathcal{L}_{\rm int}$, is $8.60\pm0.33\,{\rm pb}^{-1}$ and $\kappa = 1.86\%$ is the efficiency of the hardware trigger. The integrated luminosity of the dataset is evaluated from the number of visible pp collisions and a constant of proportionality that is measured in a dedicated calibration dataset. The absolute luminosity for the calibration dataset is determined from the beam currents, which are measured by LHC instruments, and the beam profiles and overlap integral, which are measured with a beam-gas imaging method [38]. In contrast to Ref. [38], no van der Meer scan is used. The correlation coefficient between the uncertainties of the luminosity measurements at $\sqrt{s} = 5\,{\rm TeV}$ and $\sqrt{s} = 13\,{\rm TeV}$ is 32%.

The values for the branching fractions, taken from Ref. [39], are identical to those used in the $\sqrt{s} = 13\,{\rm TeV}$ measurement [22], thus ensuring a complete cancellation in ratios between cross-sections measured at 13 and 5 TeV. The values $\mathcal{B}(D^+\to K^-\pi^+\pi^+)$, $\mathcal{B}(D^{*+}\to D^0(\to K^-\pi^+)\pi^+)$, and $\mathcal{B}(D^0\to K^\mp\pi^\pm)$ are $(9.13\pm0.19)\%$, $(2.63\pm0.04)\%$, and $(3.89\pm0.05)\%$, respectively. For the D_s^+ measurement the fraction of $D_s^+\to K^-K^+\pi^+$ decays with a K^-K^+ invariant mass in the range $1000 < m_{K^-K^+} < 1040\,{\rm MeV}/c^2$ is taken as $(2.24\pm0.13)\%$ [40].

Several sources of systematic uncertainty are identified and evaluated for each decay mode and $(p_{\rm T}, y)$ bin as described in Ref. [22]. For all decay modes, the dominant uncertainties in most bins are due to the luminosity and the estimation of the tracking efficiencies. The calibration of the tracking efficiencies is performed independently for datasets taken at different centre-of-mass energies, leading to different relative uncertainties compared to the $\sqrt{s} = 13\,{\rm TeV}$ analysis. The simulated sample gives rise to systematic uncertainties due to its finite size and imperfect modelling of the selection variables. Uncertainties are also evaluated for the PID calibration procedure to account for the finite size of the calibration sample and residual differences of the kinematic distributions between the calibration sample and the final state tracks. Additionally, an uncertainty is evaluated to account for the choice of fit models used in the determination of the signal yields. Table 2 lists the fractional systematic uncertainties for the different decay modes and their correlations between different $(p_{\rm T}, y)$ bins and decay modes.

The measured differential cross-sections are tabulated in Appendix A. Figures 5 and 6 show the D^0, D^+, D_s^+, and D^{*+} cross-section measurements and predictions [1–3], which are discussed in Sec. 6.

Table 2: Fractional systematic uncertainties, in percent. Uncertainties that are computed bin-by-bin are expressed as ranges giving the minimum to maximum values. Ranges for the correlations between p_{T}-y bins and between modes are also given, expressed in percent.

	Uncertainties (%)				Correlations (%)	
	D^0	D^+	D_s^+	D^{*+}	Bins	Decay modes
Luminosity			3.8		100	100
Tracking	3–5	5–7	4–7	5–7	90–100	90–100
Branching fractions	1.2	2.1	5.8	1.5	100	0–95
Simulation sample size	0–10	0–10	2–9	1–10	0	0
Simulation modelling	0.3	0.7	0.6	2	0	0
PID sample size	0–1	0–1	0–2	0–2	0–100	0–100
PID binning	0–30	0–10	0–20	0–20	0	0
Fit model shapes	0–3	0–3	0–3	0.0–1.0	0	0

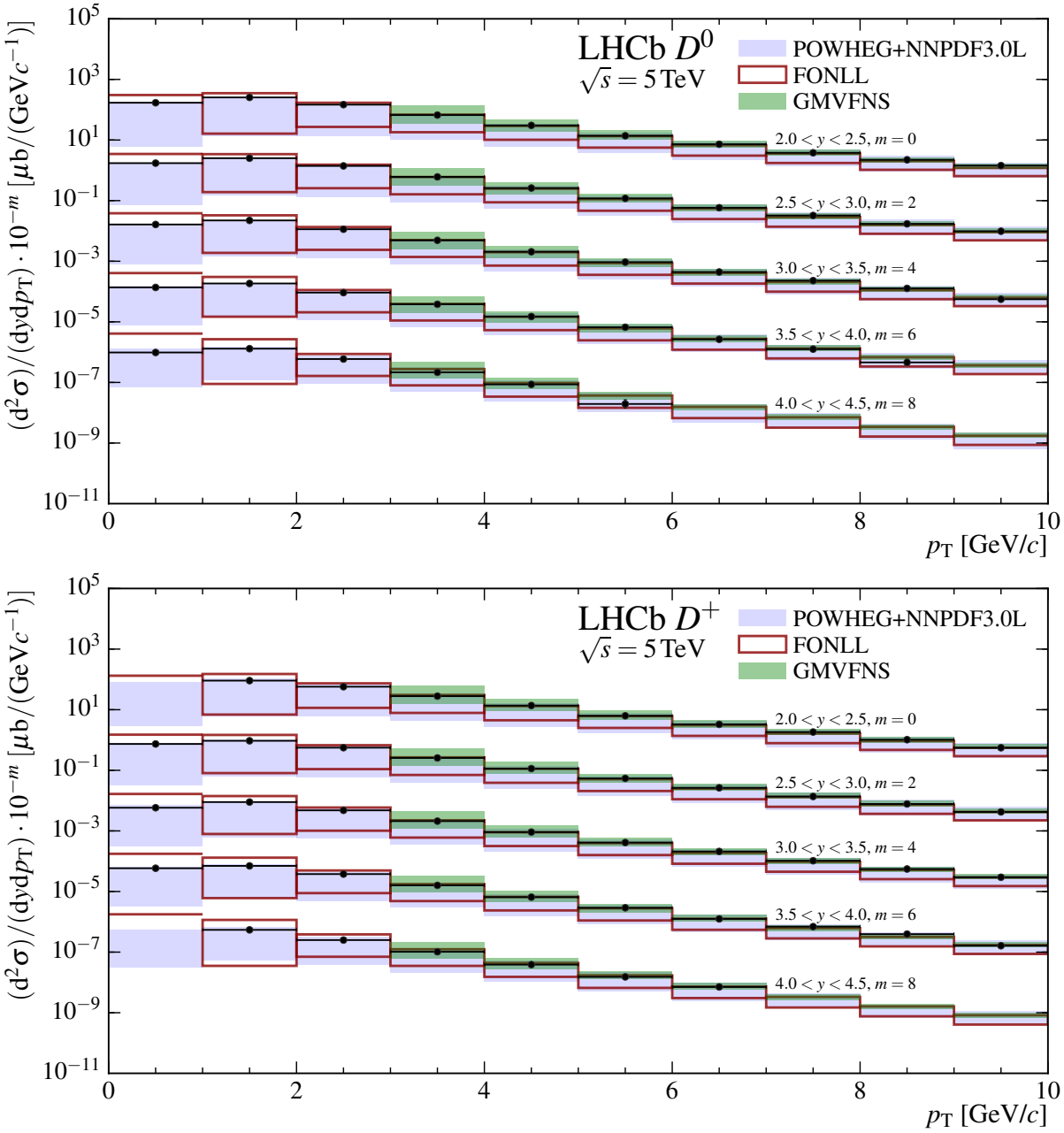

Figure 5: Measurements and predictions for the absolute prompt (top) D^0, and (bottom) D^+ cross-sections at $\sqrt{s} = 5\,\text{TeV}$. Each set of measurements and predictions in a given rapidity bin is offset by a multiplicative factor 10^{-m}, where the factor m is shown on the plots. The boxes indicate the $\pm 1\sigma$ uncertainty band on the theory predictions, where only the upper edge is shown if the uncertainty exceeds two orders of magnitude.

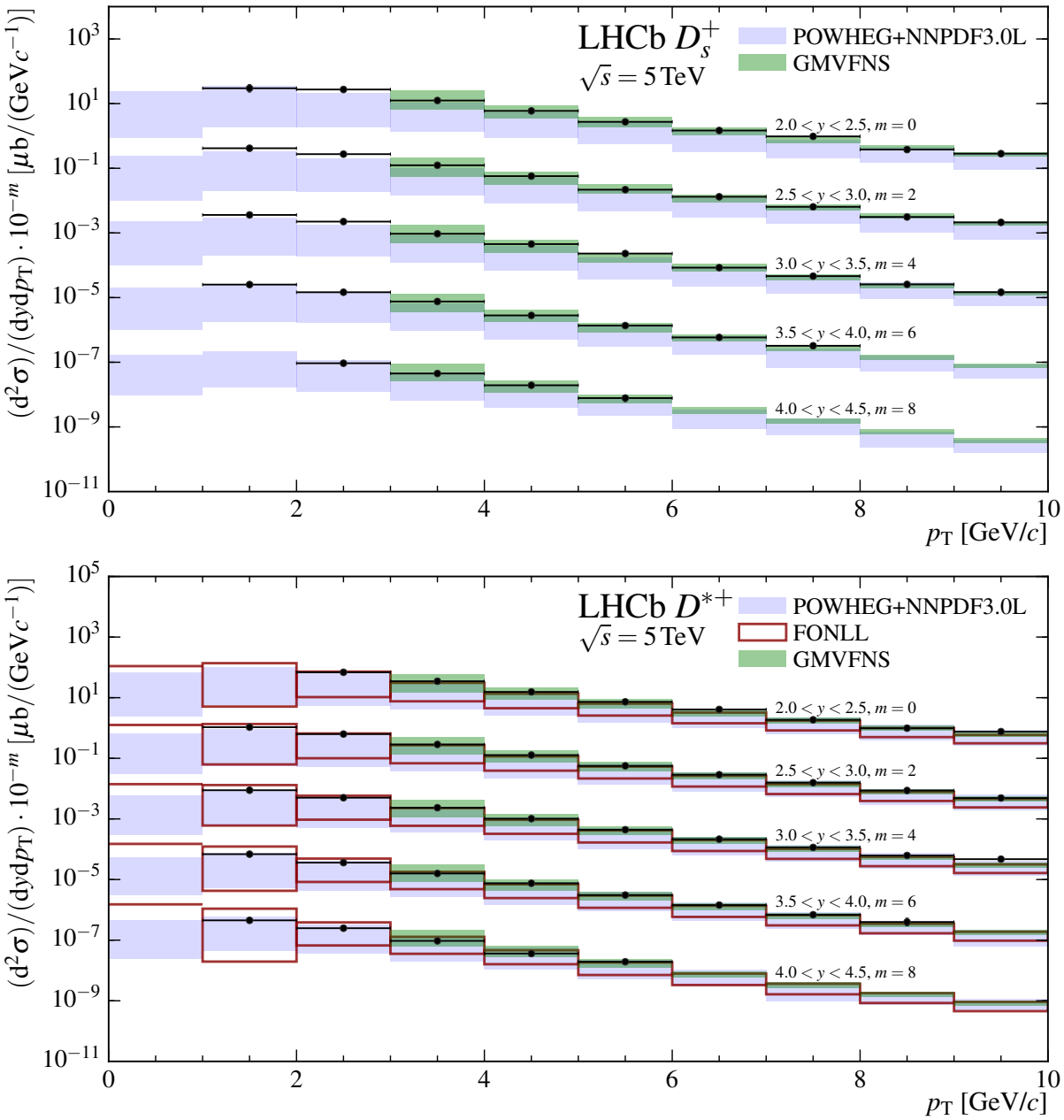

Figure 6: Measurements and predictions for the absolute prompt (top) D_s^+, and (bottom) D^{*+} cross-sections at $\sqrt{s} = 5\,\text{TeV}$. Each set of measurements and predictions in a given rapidity bin is offset by a multiplicative factor 10^{-m}, where the factor m is shown on the plots. The boxes indicate the $\pm 1\sigma$ uncertainty band on the theory predictions, where only the upper edge is shown if the uncertainty exceeds two orders of magnitude.

5 Production ratios and integrated cross-sections

5.1 Production ratios

The present analysis uses the same techniques as the LHCb measurement at $\sqrt{s} = 13\,\text{TeV}$. Therefore, several sources of systematic uncertainty are highly correlated, leading to cross-section ratios between $\sqrt{s} = 13\,\text{TeV}$ and $\sqrt{s} = 5\,\text{TeV}$, $R_{13/5}$, with greatly reduced relative uncertainties compared to the differential cross-sections. Furthermore, the predicted ratios of prompt charm production cross-sections between different centre-of-mass energies have cancellations of several theoretical uncertainties [1–3]. The $\sqrt{s} = 13\,\text{TeV}$ measurements are rebinned to match the binning used for the present results and the production ratios are presented for $0 < p_\text{T} < 8\,\text{GeV}/c$ and $2.0 < y < 4.5$ in Appendix B. Figure 7 shows the measured ratios for D^0, D^+, D_s^+, and D^{*+} mesons compared with predictions from theory calculations [1–3], discussed in Sec. 6.

A second set of differential ratios is obtained by dividing the prompt charm production cross-sections of different charm mesons. These can be compared with the ratios of the cross-sections measured at e^+e^- colliders operating at a centre-of-mass energy close to the $\Upsilon(4S)$ resonance [41–43]. Those measurements were performed with the same final states as the analysis presented here. Therefore, a more precise comparison is made by taking ratios of $\sigma(D) \times \mathcal{B}(D \to f)$. Differential ratios are shown in Figs. 8 and 9, and tabulated results are presented in Appendix C. The measurements in each p_T bin are shown integrated over y for clearer visualisation. They exhibit a p_T dependence that is consistent with heavier particles having a harder p_T spectrum.

5.2 Integrated cross-sections

Integrated production cross-sections, $\sigma(D)$, for each charm meson are computed as the sum of the measurements in each bin, where the uncertainty on the sum takes into account the correlations between bins. Integrated cross-sections are computed for all four mesons in the kinematic region $1 < p_\text{T} < 8\,\text{GeV}/c$ and $2.0 < y < 4.5$ and additionally down to $p_\text{T} = 0\,\text{GeV}/c$ for D^0 and D^+. The upper limit of $p_\text{T} = 8\,\text{GeV}/c$ is chosen to match that of the measurements at $\sqrt{s} = 7\,\text{TeV}$ and $\sqrt{s} = 13\,\text{TeV}$.

Contributions from bins within the integration range for which a measurement was not possible are estimated using a theory-based correction factor, computed as the ratio between the predicted integrated cross-section within the considered kinematic region and the sum of all cross-section predictions for bins for which a measurement exists, as in Ref. [22]. POWHEG+NNPDF3.0L [1] predictions, discussed in the next section, are used to compute the extrapolation factor. From the differences between the central value and the upper and lower bounds on the prediction, the larger of the two is assigned as systematic uncertainty of the extrapolation factor. Table 3 gives the integrated cross-sections for D^0, D^+, D_s^+, and D^{*+} mesons and Table 4 gives the corresponding values for the ratios of integrated cross-sections measured at $\sqrt{s} = 13\,\text{TeV}$ and $5\,\text{TeV}$.

The integrated $c\bar{c}$ production cross-section, $\sigma(pp \to c\bar{c}X)$, is calculated as $\sigma(D)/(2f(c \to D))$ for each decay mode. The term $f(c \to D)$ is the quark-to-hadron transition probability, and the factor 2 accounts for the inclusion of charge-conjugate states in the measurement. Measurements at e^+e^- colliders operating at a centre-of-mass energy close to the $\Upsilon(4S)$ resonance are used to determine

Table 3: Prompt D-meson production cross-sections in the kinematic ranges given. The computation of the extrapolation factors is described in Ref [22]. The first uncertainty on the cross-section is statistical, and the second is systematic and includes the contribution from the extrapolation factor. A dash indicates that measurements are available in all bins and no extrapolation factor is needed. Integrated numbers in the reduced acceptance $2.5 < y < 4.0$ are quoted as reference for future heavy ion measurements.

			Extrapolation factor	Cross-section (µb)
D^0	$0 < p_{\rm T} < 8\,{\rm GeV}/c$	$2 < y < 4.5$	1.0013 ± 0.0019	$1374 \pm 3 \pm 74$
D^+	$0 < p_{\rm T} < 8\,{\rm GeV}/c$	$2 < y < 4.5$	1.108 ± 0.049	$551 \pm 5 \pm 48$
D^0	$1 < p_{\rm T} < 8\,{\rm GeV}/c$	$2 < y < 4.5$	1.0017 ± 0.0020	$1004 \pm 3 \pm 54$
D^+	$1 < p_{\rm T} < 8\,{\rm GeV}/c$	$2 < y < 4.5$	1.00062 ± 0.00099	$402 \pm 2 \pm 30$
D_s^+	$1 < p_{\rm T} < 8\,{\rm GeV}/c$	$2 < y < 4.5$	1.0734 ± 0.0080	$170 \pm 4 \pm 16$
D^{*+}	$1 < p_{\rm T} < 8\,{\rm GeV}/c$	$2 < y < 4.5$	1.122 ± 0.046	$421 \pm 5 \pm 36$
D^0	$0 < p_{\rm T} < 8\,{\rm GeV}/c$	$2.5 < y < 4$	—	$866 \pm 2 \pm 45$
D^+	$0 < p_{\rm T} < 8\,{\rm GeV}/c$	$2.5 < y < 4$	—	$349 \pm 4 \pm 27$
D^0	$1 < p_{\rm T} < 8\,{\rm GeV}/c$	$2.5 < y < 4$	—	$630 \pm 2 \pm 33$
D^+	$1 < p_{\rm T} < 8\,{\rm GeV}/c$	$2.5 < y < 4$	—	$253 \pm 1 \pm 18$
D_s^+	$1 < p_{\rm T} < 8\,{\rm GeV}/c$	$2.5 < y < 4$	—	$110 \pm 2 \pm 10$
D^{*+}	$1 < p_{\rm T} < 8\,{\rm GeV}/c$	$2.5 < y < 4$	—	$267 \pm 3 \pm 21$

the transition probabilities [44] $f(c \to D^0) = 0.565 \pm 0.032$, $f(c \to D^+) = 0.246 \pm 0.020$, $f(c \to D_s^+) = 0.080 \pm 0.017$, and $f(c \to D^{*+}) = 0.224 \pm 0.028$. The fragmentation fraction $f(c \to D^0)$ has an overlapping contribution from $f(c \to D^{*+})$.

The combination of the individual D^0 and D^+ measurements of the $c\bar{c}$ cross-section is performed by means of a weighted average that minimises the variance of the estimate [45], giving

$$\sigma(pp \to c\bar{c}X)_{p_{\rm T} < 8\,{\rm GeV}/c,\, 2.0 < y < 4.5} = 1193 \pm 3 \pm 67 \pm 58\,{\rm \mu b},$$

where the uncertainties are due to statistical, systematic and fragmentation fraction uncertainties, respectively. The specified kinematic range refers to the produced charm hadron, not the individual charm quarks. A comparison with predictions is given in Fig. 10. The same Figure also shows a comparison of $\sigma(pp \to c\bar{c}X)$ for $1 < p_{\rm T} < 8\,{\rm GeV}/c$ based on the measurements of the four meson species. Ratios of the integrated measurements of cross-section times branching fraction are given in Table 5.

6 Comparison to theory

Theoretical calculations for charm meson production cross-sections in pp collisions at $\sqrt{s} = 5\,{\rm TeV}$, according to the same methods described in Refs. [1] (POWHEG+NNPDF3.0L), [2] (FONLL) and [3] (GMVFNS), have been provided by the authors. All sets of calculations are performed at NLO precision, and each includes estimates of theoretical uncertainties due to the renormalisation and factorisation scales. The theoretical uncertainties provided with the POWHEG+NNPDF3.0L predictions also

Table 4: Ratios of integrated prompt D-meson production cross-sections between measurements at $\sqrt{s} = 13\,\text{TeV}$ and $\sqrt{s} = 5\,\text{TeV}$. The first uncertainty on the ratio is statistical, and the second is systematic.

			$R_{13/5}$
D^0	$0 < p_\text{T} < 8\,\text{GeV}/c$	$2 < y < 4.5$	$1.977 \pm 0.005 \pm 0.120$
D^+	$0 < p_\text{T} < 8\,\text{GeV}/c$	$2 < y < 4.5$	$2.02 \pm 0.02 \pm 0.22$
D^0	$1 < p_\text{T} < 8\,\text{GeV}/c$	$2 < y < 4.5$	$2.070 \pm 0.006 \pm 0.121$
D^+	$1 < p_\text{T} < 8\,\text{GeV}/c$	$2 < y < 4.5$	$2.09 \pm 0.01 \pm 0.19$
D_s^+	$1 < p_\text{T} < 8\,\text{GeV}/c$	$2 < y < 4.5$	$2.09 \pm 0.07 \pm 0.23$
D^{*+}	$1 < p_\text{T} < 8\,\text{GeV}/c$	$2 < y < 4.5$	$1.87 \pm 0.03 \pm 0.23$

Table 5: Ratios of the measurements of cross-section times branching fraction in the kinematic range $1 < p_\text{T} < 8\,\text{GeV}/c$ and $2 < y < 4.5$. The first uncertainty on the ratio is statistical and the second is systematic. The notation $\sigma(D \to f)$ is shorthand for $\sigma(D) \times \mathcal{B}(D \to f)$.

Quantity	Measurement
$\sigma(D^+ \to K^-\pi^+\pi^+)/\sigma(D^0 \to K^-\pi^+)$	$0.943^{+\ 0.005+\ 0.029}_{-\ 0.005-\ 0.029}$
$\sigma(D_s^+ \to [K^-K^+]_\phi\pi^+)/\sigma(D^0 \to K^-\pi^+)$	$0.0983^{+0.0021+0.0035}_{-0.0021-0.0035}$
$\sigma(D^{*+} \to [K^-\pi^+]_{D^0}\pi^+)/\sigma(D^0 \to K^-\pi^+)$	$0.283^{+\ 0.004+\ 0.016}_{-\ 0.004-\ 0.016}$
$\sigma(D_s^+ \to [K^-K^+]_\phi\pi^+)/\sigma(D^+ \to K^-\pi^+\pi^+)$	$0.1042^{+0.0022+0.0031}_{-0.0022-0.0031}$
$\sigma(D^{*+} \to [K^-\pi^+]_{D^0}\pi^+)/\sigma(D^+ \to K^-\pi^+\pi^+)$	$0.300^{+\ 0.004+\ 0.015}_{-\ 0.004-\ 0.015}$
$\sigma(D_s^+ \to [K^-K^+]_\phi\pi^+)/\sigma(D^{*+} \to [K^-\pi^+]_{D^0}\pi^+)$	$0.348^{+\ 0.008+\ 0.018}_{-\ 0.009-\ 0.018}$

include contributions due to uncertainties in the effective charm quark mass and the parton distribution functions.

The FONLL predictions are provided in the form of D^0, D^+, and D^{*+} production cross-sections for pp collisions at $\sqrt{s} = 5\,\text{TeV}$ for each phase space bin in the range $p_\text{T} < 10\,\text{GeV}/c$ and $2.0 < y < 4.5$. Ratios of these cross-sections to those computed for pp collisions at 13 TeV are also supplied. The calculations use the NNPDF3.0 NLO [46] parton densities. These FONLL calculations of the meson differential production cross-sections assume $f(c \to D) = 1$ and are multiplied by the transition probabilities measured at e^+e^- colliders for comparison to the current measurements. No dedicated FONLL cross-section calculation for D_s^+ production is available.

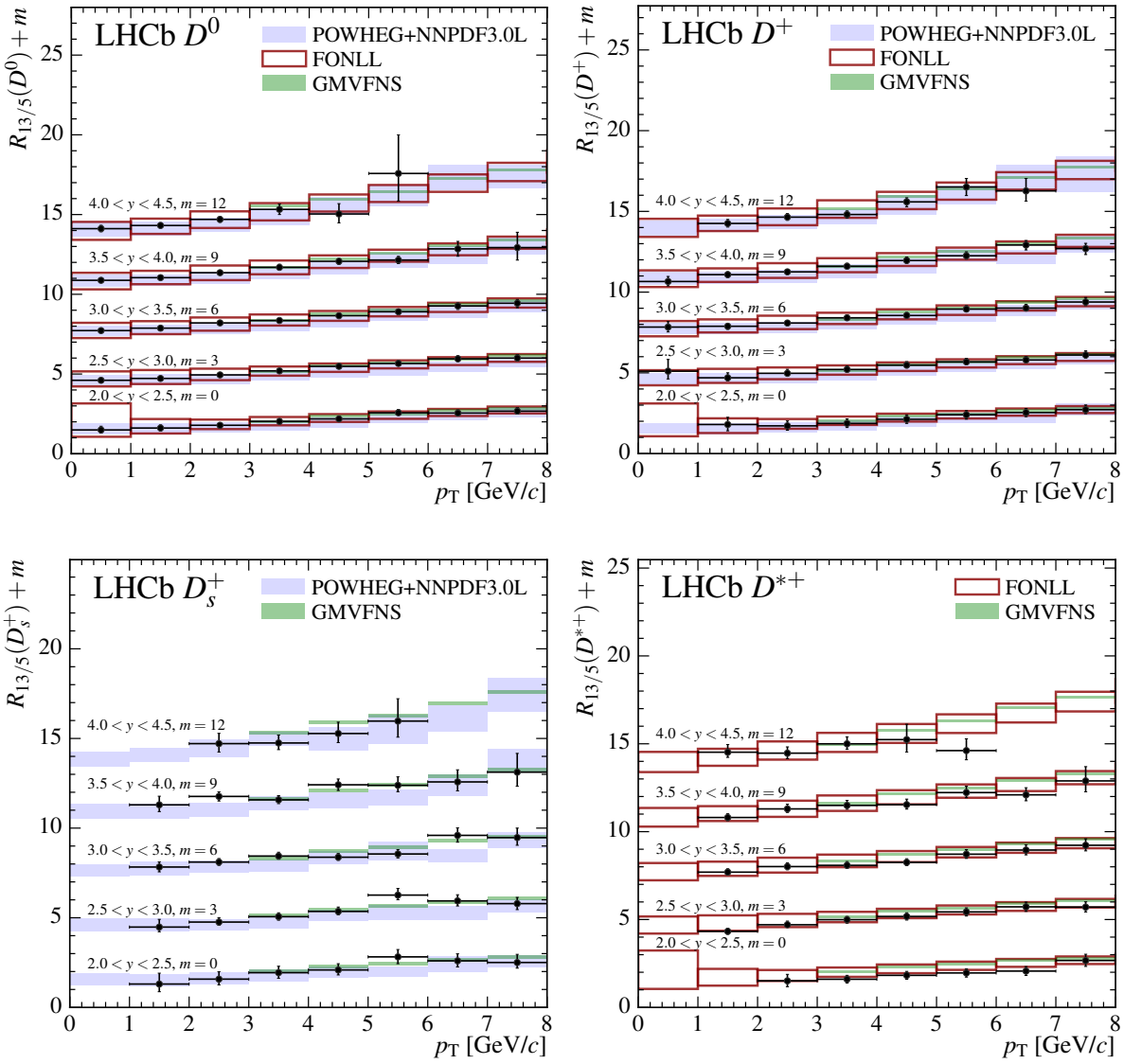

Figure 7: Measurements and predictions of the prompt D^0, D^+, D_s^+, and D^{*+} cross-section ratios between $\sqrt{s} = 13$ and 5 TeV. Each set of measurements and predictions in a given rapidity bin is offset by an additive constant m, which is shown on the plot. Only central values are provided for the GMVFNS predictions.

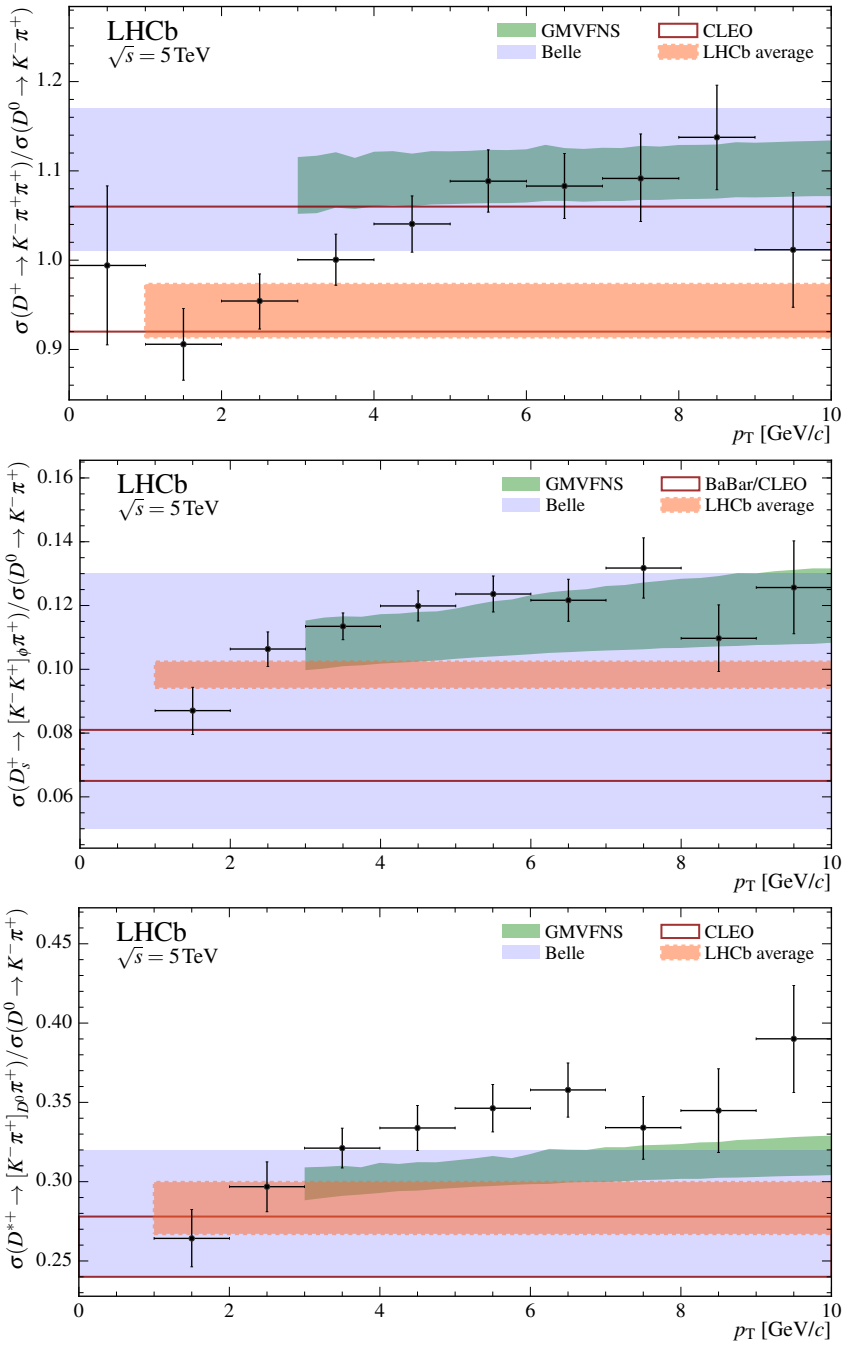

Figure 8: Ratios of the measurements of cross-section times branching fraction of (top) D^+, (middle) D_s^+, and (bottom) D^{*+} mesons with respect to the D^0 measurements. The bands indicate the corresponding ratios computed using measurements from e^+e^- collider experiments [41–43]. The ratios are given as a function of $p_{\rm T}$ integrated over y. The notation $\sigma(D \to f)$ is shorthand for $\sigma(D) \times \mathcal{B}(D \to f)$.

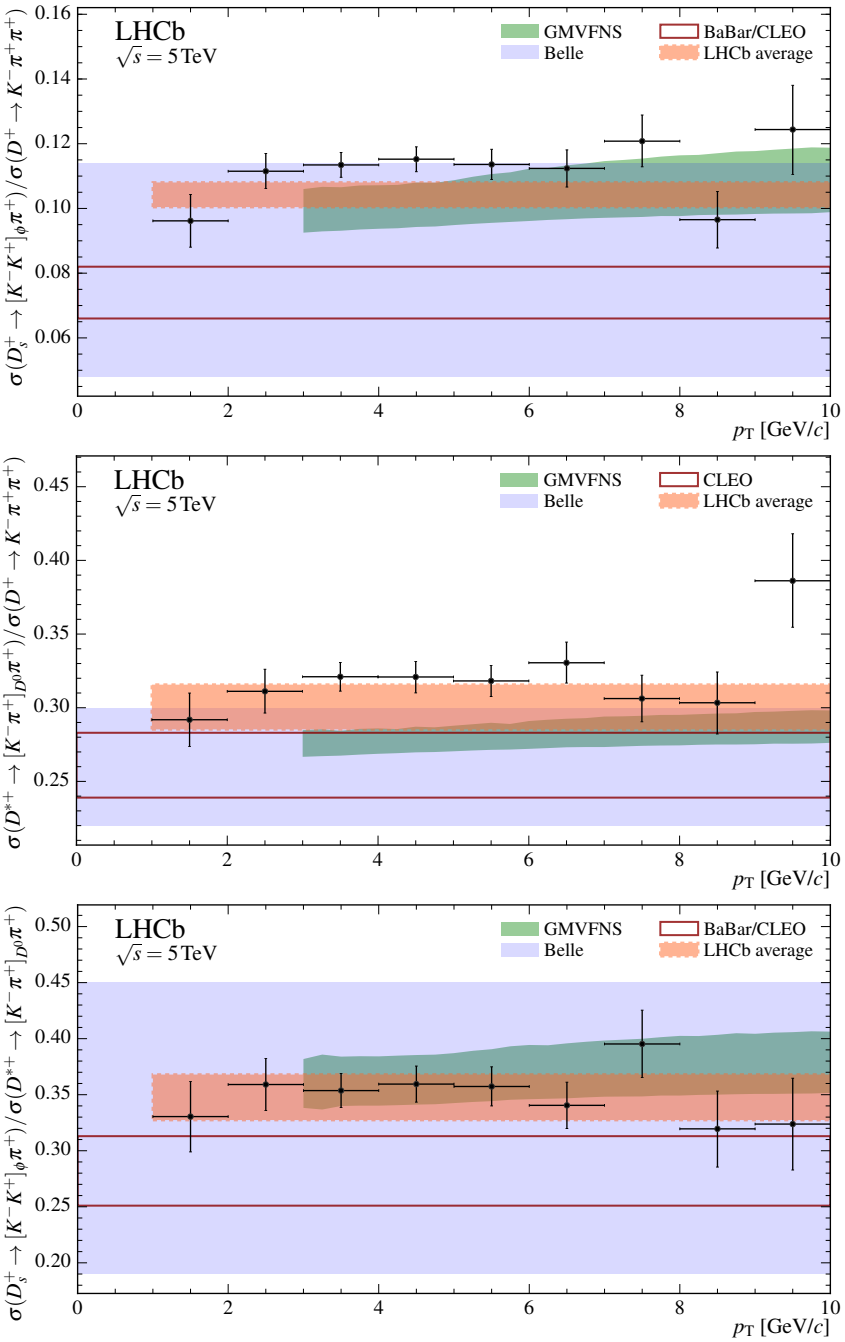

Figure 9: Ratios of the measurements of cross-section times branching fraction of (top) D^{*+}, and (middle) D_s^+ mesons with respect to D^+ cross-sections, and (bottom) D_s^+ over D^{*+} mesons. The bands indicate the corresponding ratios computed using measurements from e^+e^- collider experiments [41–43]. The ratios are given as a function of p_T integrated over y. The notation $\sigma(D \to f)$ is shorthand for $\sigma(D) \times \mathcal{B}(D \to f)$.

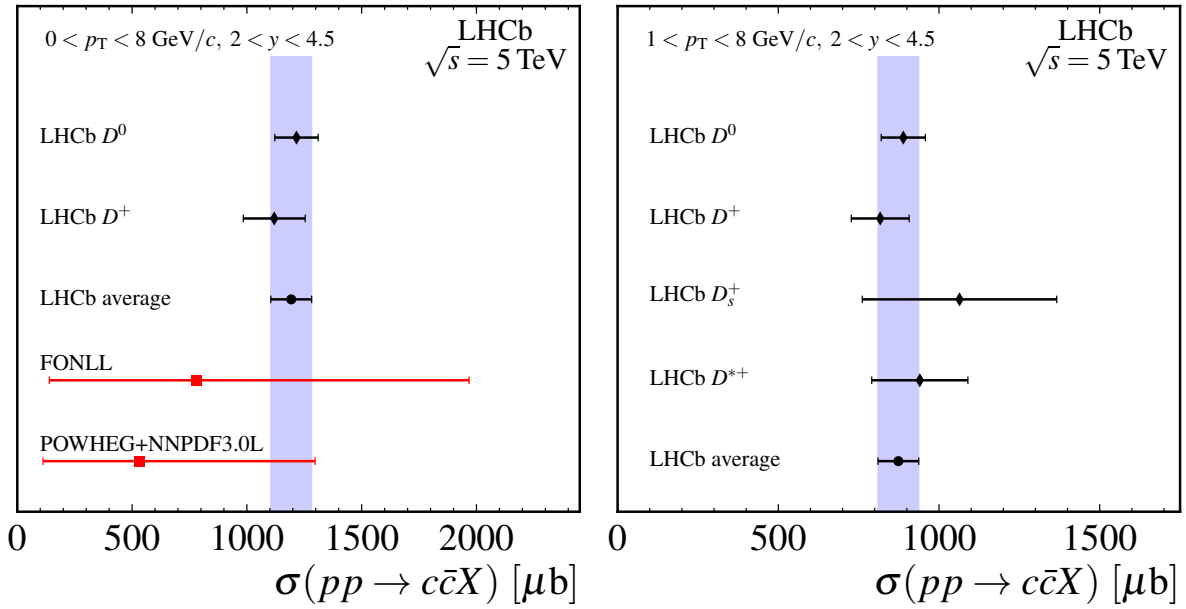

Figure 10: Integrated $c\bar{c}$ cross-sections (black diamonds), their average (black circle and blue band) and theory predictions (red squares) [1, 2] are shown (left) based on the D^0 and D^+ for $0 < p_T < 8\,\text{GeV}/c$ and (right) for measurements based on all four mesons for $1 < p_T < 8\,\text{GeV}/c$.

The POWHEG+NNPDF3.0L predictions provide D^0, D^+, and D_s^+ integrated production cross-sections for pp collisions at $\sqrt{s} = 5\,\text{TeV}$ in the same p_T and y binning used for the measurement. Ratios of $\sqrt{s} = 13\,\text{TeV}$ to $5\,\text{TeV}$ cross-sections are also predicted for D^0, D^+ and D_s^+. They are obtained with POWHEG [47] matched to PYTHIA8 [48] parton showers and an improved version of the NNPDF3.0 NLO parton distribution function set designated NNPDF3.0+LHCb [1]. To produce this improved set, the authors of Ref. [1] weight the NNPDF3.0 NLO set in order to match FONLL calculations to the LHCb charm cross-section measurements at 7 TeV [21]. This results in a significant reduction in the uncertainties for the gluon distribution function at small momentum fraction x. Predictions for the integrated cross-section are provided for each meson.

The GMVFNS calculations include theoretical predictions for the absolute cross-sections for all mesons studied in this analysis. Predictions of central values are also provided for the cross-section ratios between mesons. Results are provided for $3 < p_T < 10\,\text{GeV}/c$. Here the CT10 [49] set of parton distributions is used. The GMVFNS theoretical framework includes the convolution with fragmentation functions describing the transition $c \to D$ that are normalised to the respective total transition probabilities [8, 50]. The fragmentation functions are taken from a fit to production measurements at e^+e^- colliders, where no attempt is made to separate direct production and feed-down from higher resonances.

In general, the predicted shapes of the cross-sections at $\sqrt{s} = 5\,\text{TeV}$ agree with the data shown in Figures 5 and 6. The central values of the measurements generally lie above those of the theory predictions, albeit within the uncertainties provided. For the POWHEG+NNPDF3.0L and FONLL predictions, the data tend to lie at the upper edge of the uncertainty band. The GMVFNS predictions provide a better description of the data, although the cross-sections decrease with p_T at a higher rate than the data near their low p_T limit of $3\,\text{GeV}/c$. Similar behaviour was observed for the $\sqrt{s} = 7\,\text{TeV}$ measurement [21],

where only central values were shown for the FONLL prediction, and for the $\sqrt{s} = 13\,\text{TeV}$ measurement [22], where in both cases the predictions gave lower cross-sections than the data.

The data generally agree well with the FONLL, POWHEG+NNPDF3.0L and GMVFNS predictions for the ratios of cross-sections at $\sqrt{s} = 13\,\text{TeV}$ and 5 TeV, shown in Figure 7. These ratio measurements are significantly more precise than those previously presented between cross-sections at $\sqrt{s} = 13\,\text{TeV}$ and 7 TeV, and will act as stronger constraints in PDF fits as a result.

7 Summary

A measurement of charm production in pp collisions at a centre-of-mass energy of $\sqrt{s} = 5\,\text{TeV}$ has been performed with data collected with the LHCb detector. While the shapes of the differential cross-sections for D^0, D^+, D_s^+, and D^{*+} mesons are found to be in agreement with NLO perturbative QCD calculations, the measured values tend to lie at the upper edge of the predictions. This is a feature also common to the measurements at $\sqrt{s} = 7$ and 13 TeV, which indicates a general underestimation in the prediction of the absolute value of prompt charm production in the forward region. The ratios of the production cross-sections for centre-of-mass energies of 13 TeV and 5 TeV have been measured and show consistency with theoretical predictions. The integrated cross-sections for prompt open charm meson production in pp collisions at $\sqrt{s} = 5\,\text{TeV}$ and in the range $1 < p_\text{T} < 8\,\text{GeV}/c$ and $2 < y < 4.5$ are

$$\begin{aligned}
\sigma(pp \to D^0 X) &= 1004 \pm 3 \pm 54\,\mu\text{b}, \\
\sigma(pp \to D^+ X) &= 402 \pm 2 \pm 30\,\mu\text{b}, \\
\sigma(pp \to D_s^+ X) &= 170 \pm 4 \pm 16\,\mu\text{b}, \\
\sigma(pp \to D^{*+} X) &= 421 \pm 5 \pm 36\,\mu\text{b}.
\end{aligned}$$

Acknowledgements

The authors would like to thank R. Gauld and J. Rojo for the provisions of the POWHEG+NNPDF3.0L numbers; M. Cacciari, M.L. Mangano, and P. Nason for the FONLL predictions; and H. Spiesberger and G. Kramer for the GMVFNS calculations. We express our gratitude to our colleagues in the CERN accelerator departments for the excellent performance of the LHC. We thank the technical and administrative staff at the LHCb institutes. We acknowledge support from CERN and from the national agencies: CAPES, CNPq, FAPERJ and FINEP (Brazil); NSFC (China); CNRS/IN2P3 (France); BMBF, DFG and MPG (Germany); INFN (Italy); FOM and NWO (The Netherlands); MNiSW and NCN (Poland); MEN/IFA (Romania); MinES and FASO (Russia); MinECo (Spain); SNSF and SER (Switzerland); NASU (Ukraine); STFC (United Kingdom); NSF (USA). We acknowledge the computing resources that are provided by CERN, IN2P3 (France), KIT and DESY (Germany), INFN (Italy), SURF (The Netherlands), PIC (Spain), GridPP (United Kingdom), RRCKI and Yandex LLC (Russia), CSCS (Switzerland), IFIN-HH (Romania), CBPF (Brazil), PL-GRID (Poland) and OSC (USA). We are indebted to the communities behind the multiple open source software packages on which we depend. Individual groups or members have received support from AvH Foundation

(Germany), EPLANET, Marie Skłodowska-Curie Actions and ERC (European Union), Conseil Général de Haute-Savoie, Labex ENIGMASS and OCEVU, Région Auvergne (France), RFBR and Yandex LLC (Russia), GVA, XuntaGal and GENCAT (Spain), Herchel Smith Fund, The Royal Society, Royal Commission for the Exhibition of 1851 and the Leverhulme Trust (United Kingdom).

Appendices

A Absolute cross-sections

Tables 6–9 give the numerical results for the differential cross-sections.

Table 6: Differential production cross-sections, $\mathrm{d}^2\sigma/(\mathrm{d}p_\mathrm{T}\,\mathrm{d}y)$, in μb/(GeV/c) for prompt $D^0 + \overline{D}^0$ mesons in bins of (p_T, y). The first uncertainty is statistical, and the second is the total systematic.

p_T [GeV/c]	y			
	$[2.0, 2.5]$	$[2.5, 3.0]$	$[3.0, 3.5]$	$[3.5, 4.0]$	$[4.0, 4.5]$
$[0, 1]$	$170^{+\ 19}_{-\ 17}$	$173^{+\ 10}_{-\ 10}$	$163.1^{+\ 8.6}_{-\ 9.2}$	$136.5^{+\ 8.2}_{-\ 7.4}$	$97.3^{+\ 8.0}_{-\ 7.1}$
$[1, 2]$	$255^{+\ 21}_{-\ 19}$	$252^{+\ 13}_{-\ 15}$	$222^{+\ 11}_{-\ 12}$	$184^{+\ 10}_{-\ 10}$	$130.1^{+\ 8.2}_{-\ 7.9}$
$[2, 3]$	$147.0^{+\ 9.4}_{-\ 9.1}$	$139.7^{+\ 6.8}_{-\ 8.1}$	$113.7^{+\ 6.1}_{-\ 5.9}$	$92.2^{+\ 5.2}_{-\ 5.1}$	$59.2^{+\ 3.5}_{-\ 3.4}$
$[3, 4]$	$66.7^{+\ 3.9}_{-\ 3.7}$	$60.8^{+\ 3.1}_{-\ 3.3}$	$49.0^{+\ 2.6}_{-\ 2.5}$	$37.9^{+\ 2.2}_{-\ 2.1}$	$21.6^{+\ 1.8}_{-\ 1.6}$
$[4, 5]$	$30.4^{+\ 1.6}_{-\ 1.8}$	$26.0^{+\ 1.4}_{-\ 1.4}$	$20.5^{+\ 1.2}_{-\ 1.0}$	$14.96^{+\ 0.85}_{-\ 0.77}$	$8.6^{+\ 1.5}_{-\ 1.1}$
$[5, 6]$	$13.83^{+\ 0.74}_{-\ 0.79}$	$11.84^{+\ 0.61}_{-\ 0.67}$	$9.34^{+\ 0.58}_{-\ 0.47}$	$6.62^{+\ 0.46}_{-\ 0.39}$	$1.95^{+\ 0.67}_{-\ 0.41}$
$[6, 7]$	$7.25^{+\ 0.40}_{-\ 0.42}$	$5.83^{+\ 0.32}_{-\ 0.34}$	$4.41^{+\ 0.27}_{-\ 0.22}$	$2.65^{+\ 0.28}_{-\ 0.22}$	
$[7, 8]$	$3.80^{+\ 0.22}_{-\ 0.23}$	$3.23^{+\ 0.21}_{-\ 0.18}$	$2.29^{+\ 0.16}_{-\ 0.13}$	$1.26^{+\ 0.25}_{-\ 0.18}$	
$[8, 9]$	$2.23^{+\ 0.15}_{-\ 0.15}$	$1.71^{+\ 0.12}_{-\ 0.11}$	$1.27^{+\ 0.12}_{-\ 0.10}$	$0.46^{+\ 0.11}_{-\ 0.08}$	
$[9, 10]$	$1.43^{+\ 0.10}_{-\ 0.11}$	$0.978^{+\ 0.076}_{-\ 0.066}$	$0.556^{+\ 0.077}_{-\ 0.060}$		

Table 7: Differential production cross-sections, $\mathrm{d}^2\sigma/(\mathrm{d}p_\mathrm{T}\,\mathrm{d}y)$, in µb/(GeV/$c$) for prompt $D^+ + D^-$ mesons in bins of (p_T, y). The first uncertainty is statistical, and the second is the total systematic.

	y				
p_T [GeV/c]	[2.0, 2.5]	[2.5, 3.0]	[3.0, 3.5]	[3.5, 4.0]	[4.0, 4.5]
[0, 1]		$74 \pm 7 \pm 10 \pm 11$	$58.2 \pm 3.5 \pm 7.0 \pm 6.0$	$58.6 \pm 4.1 \pm 6.9 \pm 6.1$	
[1, 2]	$91 \pm 3 \pm 14 \pm 12$	$94.3 \pm 1.0 \pm 7.4 \pm 8.4$	$89.6 \pm 0.8 \pm 8.0 \pm 6.5$	$70.1 \pm 0.8 \pm 5.6 \pm 4.7$	$54.2 \pm 1.3 \pm 4.9 \pm 4.5$
[2, 3]	$57.4 \pm 0.8 \pm 6.2 \pm 5.7$	$55.8 \pm 0.4 \pm 3.7 \pm 4.7$	$47.7 \pm 0.3 \pm 3.7 \pm 3.1$	$37.6 \pm 0.3 \pm 2.9 \pm 2.4$	$25.0 \pm 0.4 \pm 1.9 \pm 1.9$
[3, 4]	$28.0 \pm 0.4 \pm 2.4 \pm 2.5$	$25.6 \pm 0.2 \pm 1.5 \pm 2.1$	$21.0 \pm 0.1 \pm 1.4 \pm 1.4$	$16.0 \pm 0.1 \pm 1.1 \pm 1.1$	$10.26 \pm 0.19 \pm 0.82 \pm 0.77$
[4, 5]	$13.7 \pm 0.2 \pm 1.0 \pm 1.2$	$11.39 \pm 0.10 \pm 0.71 \pm 0.84$	$9.15 \pm 0.09 \pm 0.62 \pm 0.61$	$6.52 \pm 0.08 \pm 0.44 \pm 0.43$	$3.86 \pm 0.11 \pm 0.30 \pm 0.26$
[5, 6]	$6.30 \pm 0.11 \pm 0.45 \pm 0.49$	$5.41 \pm 0.06 \pm 0.34 \pm 0.39$	$4.13 \pm 0.05 \pm 0.28 \pm 0.27$	$2.90 \pm 0.05 \pm 0.20 \pm 0.20$	$1.52 \pm 0.08 \pm 0.15 \pm 0.13$
[6, 7]	$3.29 \pm 0.07 \pm 0.23 \pm 0.25$	$2.64 \pm 0.04 \pm 0.17 \pm 0.19$	$2.10 \pm 0.04 \pm 0.15 \pm 0.14$	$1.249 \pm 0.034 \pm 0.095 \pm 0.086$	$0.709 \pm 0.068 \pm 0.082 \pm 0.073$
[7, 8]	$1.83 \pm 0.05 \pm 0.13 \pm 0.15$	$1.366 \pm 0.028 \pm 0.089 \pm 0.100$	$1.037 \pm 0.025 \pm 0.073 \pm 0.072$	$0.693 \pm 0.027 \pm 0.063 \pm 0.052$	
[8, 9]	$1.025 \pm 0.033 \pm 0.072 \pm 0.081$	$0.775 \pm 0.021 \pm 0.052 \pm 0.059$	$0.554 \pm 0.019 \pm 0.044 \pm 0.039$	$0.393 \pm 0.024 \pm 0.050 \pm 0.039$	
[9, 10]	$0.555 \pm 0.023 \pm 0.043 \pm 0.046$	$0.423 \pm 0.015 \pm 0.030 \pm 0.033$	$0.295 \pm 0.013 \pm 0.029 \pm 0.023$	$0.162 \pm 0.016 \pm 0.028 \pm 0.021$	

Table 8: Differential production cross-sections, $\mathrm{d}^2\sigma/(\mathrm{d}p_\mathrm{T}\,\mathrm{d}y)$, in µb/(GeV/$c$) for prompt $D_s^+ + D_s^-$ mesons in bins of (p_T, y). The first uncertainty is statistical, and the second is the total systematic.

p_T [GeV/c]	y [2.0, 2.5]	[2.5, 3.0]	[3.0, 3.5]	[3.5, 4.0]	[4.0, 4.5]
[1, 2]	$29.8^{+\ 4.6\ +\ 7.5}_{-\ 4.6\ -\ 5.3}$	$41.6^{+\ 2.5\ +\ 4.4}_{-\ 2.5\ -\ 4.6}$	$36.0^{+\ 2.3\ +\ 4.2}_{-\ 2.2\ -\ 3.6}$	$25.3^{+\ 2.3\ +\ 3.0}_{-\ 2.3\ -\ 2.5}$	
[2, 3]	$27.3^{+\ 1.5\ +\ 5.1}_{-\ 1.5\ -\ 4.0}$	$27.4^{+\ 0.8\ +\ 2.4}_{-\ 0.8\ -\ 2.7}$	$22.4^{+\ 0.7\ +\ 2.2}_{-\ 0.7\ -\ 1.9}$	$14.6^{+\ 0.6\ +\ 1.5}_{-\ 0.6\ -\ 1.2}$	$9.3^{+\ 1.0\ +\ 1.5}_{-\ 1.0\ -\ 1.2}$
[3, 4]	$12.5^{+\ 0.6\ +\ 1.7}_{-\ 0.6\ -\ 1.4}$	$12.4^{+\ 0.4\ +\ 1.0}_{-\ 0.4\ -\ 1.1}$	$9.42^{+\ 0.30\ +\ 0.91}_{-\ 0.30\ -\ 0.75}$	$7.57^{+\ 0.32\ +\ 0.72}_{-\ 0.32\ -\ 0.61}$	$4.49^{+\ 0.42\ +\ 0.52}_{-\ 0.42\ -\ 0.42}$
[4, 5]	$5.96^{+\ 0.30\ +\ 0.59}_{-\ 0.30\ -\ 0.63}$	$5.71^{+\ 0.20\ +\ 0.48}_{-\ 0.20\ -\ 0.51}$	$4.52^{+\ 0.18\ +\ 0.43}_{-\ 0.18\ -\ 0.37}$	$2.81^{+\ 0.16\ +\ 0.28}_{-\ 0.16\ -\ 0.23}$	$1.94^{+\ 0.24\ +\ 0.25}_{-\ 0.24\ -\ 0.18}$
[5, 6]	$2.73^{+\ 0.18\ +\ 0.27}_{-\ 0.17\ -\ 0.27}$	$2.18^{+\ 0.11\ +\ 0.19}_{-\ 0.11\ -\ 0.19}$	$2.30^{+\ 0.11\ +\ 0.23}_{-\ 0.11\ -\ 0.19}$	$1.36^{+\ 0.10\ +\ 0.14}_{-\ 0.10\ -\ 0.11}$	$0.78^{+\ 0.15\ +\ 0.12}_{-\ 0.15\ -\ 0.08}$
[6, 7]	$1.47^{+\ 0.11\ +\ 0.15}_{-\ 0.11\ -\ 0.14}$	$1.31^{+\ 0.08\ +\ 0.13}_{-\ 0.08\ -\ 0.11}$	$0.843^{+\ 0.062\ +\ 0.089}_{-\ 0.062\ -\ 0.070}$	$0.586^{+\ 0.065\ +\ 0.074}_{-\ 0.065\ -\ 0.057}$	
[7, 8]	$0.97^{+\ 0.09\ +\ 0.10}_{-\ 0.09\ -\ 0.10}$	$0.642^{+\ 0.052\ +\ 0.070}_{-\ 0.052\ -\ 0.053}$	$0.461^{+\ 0.044\ +\ 0.052}_{-\ 0.044\ -\ 0.039}$	$0.323^{+\ 0.046\ +\ 0.057}_{-\ 0.046\ -\ 0.039}$	
[8, 9]	$0.379^{+\ 0.052\ +\ 0.041}_{-\ 0.052\ -\ 0.039}$	$0.311^{+\ 0.035\ +\ 0.038}_{-\ 0.035\ -\ 0.027}$	$0.256^{+\ 0.034\ +\ 0.034}_{-\ 0.034\ -\ 0.025}$		
[9, 10]	$0.284^{+\ 0.042\ +\ 0.035}_{-\ 0.042\ -\ 0.034}$	$0.212^{+\ 0.028\ +\ 0.028}_{-\ 0.028\ -\ 0.020}$	$0.147^{+\ 0.025\ +\ 0.022}_{-\ 0.025\ -\ 0.015}$		

Table 9: Differential production cross-sections, $\mathrm{d}^2\sigma/(\mathrm{d}p_\mathrm{T}\,\mathrm{d}y)$, in µb/(GeV/$c$) for prompt $D^{*+} + D^{*-}$ mesons in bins of (p_T, y). The first uncertainty is statistical, and the second is the total systematic.

	y				
p_T [GeV/c]	$[2.0, 2.5]$	$[2.5, 3.0]$	$[3.0, 3.5]$	$[3.5, 4.0]$	$[4.0, 4.5]$
$[1, 2]$		$106 \,^{+\ 5\ +\ 11}_{-\ 5\ -\ 9}$	$88.4 \,^{+\ 2.0\ +\ 7.1}_{-\ 2.0\ -\ 8.3}$	$68.7 \,^{+\ 1.9\ +\ 5.9}_{-\ 1.9\ -\ 6.3}$	$45.0 \,^{+\ 2.7\ +\ 3.9}_{-\ 2.7\ -\ 4.4}$
$[2, 3]$	$68.8 \,^{+\ 6.8\ +\ 8.1}_{-\ 6.8\ -\ 8.5}$	$63.0 \,^{+\ 1.5\ +\ 4.2}_{-\ 1.5\ -\ 5.1}$	$50.0 \,^{+\ 0.8\ +\ 3.9}_{-\ 0.8\ -\ 4.4}$	$36.1 \,^{+\ 0.8\ +\ 3.0}_{-\ 0.8\ -\ 3.3}$	$24.8 \,^{+\ 1.2\ +\ 2.9}_{-\ 1.2\ -\ 2.7}$
$[3, 4]$	$34.9 \,^{+\ 1.7\ +\ 2.8}_{-\ 1.7\ -\ 3.0}$	$28.6 \,^{+\ 0.6\ +\ 2.1}_{-\ 0.6\ -\ 2.1}$	$23.4 \,^{+\ 0.4\ +\ 2.0}_{-\ 0.4\ -\ 1.8}$	$15.8 \,^{+\ 0.4\ +\ 1.3}_{-\ 0.4\ -\ 1.4}$	$9.46 \,^{+\ 0.59\ +\ 0.72}_{-\ 0.59\ -\ 0.79}$
$[4, 5]$	$15.5 \,^{+\ 0.7\ +\ 1.2}_{-\ 0.7\ -\ 1.3}$	$12.76 \,^{+\ 0.29\ +\ 0.86}_{-\ 0.29\ -\ 0.98}$	$10.17 \,^{+\ 0.23\ +\ 0.92}_{-\ 0.23\ -\ 0.71}$	$7.53 \,^{+\ 0.24\ +\ 0.71}_{-\ 0.24\ -\ 0.70}$	$3.61 \,^{+\ 0.40\ +\ 0.82}_{-\ 0.40\ -\ 0.55}$
$[5, 6]$	$7.30 \,^{+\ 0.35\ +\ 0.55}_{-\ 0.35\ -\ 0.60}$	$5.63 \,^{+\ 0.16\ +\ 0.38}_{-\ 0.16\ -\ 0.43}$	$4.40 \,^{+\ 0.14\ +\ 0.38}_{-\ 0.14\ -\ 0.32}$	$3.07 \,^{+\ 0.15\ +\ 0.28}_{-\ 0.15\ -\ 0.22}$	$1.93 \,^{+\ 0.06\ +\ 0.31}_{-\ 0.06\ -\ 0.25}$
$[6, 7]$	$4.09 \,^{+\ 0.22\ +\ 0.30}_{-\ 0.22\ -\ 0.34}$	$2.87 \,^{+\ 0.11\ +\ 0.20}_{-\ 0.11\ -\ 0.22}$	$2.14 \,^{+\ 0.09\ +\ 0.18}_{-\ 0.09\ -\ 0.16}$	$1.43 \,^{+\ 0.10\ +\ 0.12}_{-\ 0.10\ -\ 0.12}$	
$[7, 8]$	$1.86 \,^{+\ 0.13\ +\ 0.14}_{-\ 0.13\ -\ 0.16}$	$1.57 \,^{+\ 0.08\ +\ 0.11}_{-\ 0.08\ -\ 0.12}$	$1.15 \,^{+\ 0.06\ +\ 0.10}_{-\ 0.06\ -\ 0.09}$	$0.690 \,^{+\ 0.081\ +\ 0.081}_{-\ 0.081\ -\ 0.071}$	
$[8, 9]$	$0.984 \,^{+\ 0.085\ +\ 0.079}_{-\ 0.085\ -\ 0.090}$	$0.866 \,^{+\ 0.054\ +\ 0.063}_{-\ 0.054\ -\ 0.069}$	$0.622 \,^{+\ 0.047\ +\ 0.060}_{-\ 0.047\ -\ 0.046}$	$0.40 \,^{+\ 0.07\ +\ 0.11}_{-\ 0.07\ -\ 0.07}$	
$[9, 10]$	$0.758 \,^{+\ 0.073\ +\ 0.067}_{-\ 0.073\ -\ 0.075}$	$0.488 \,^{+\ 0.040\ +\ 0.039}_{-\ 0.040\ -\ 0.042}$	$0.470 \,^{+\ 0.044\ +\ 0.064}_{-\ 0.044\ -\ 0.050}$		

B Cross-section ratios at different energies

Tables 10–13 give the numerical results of the cross-section ratios between $\sqrt{s} = 13$ and 5 TeV.

Table 10: The ratios of differential production cross-sections, $R_{13/5}$, for prompt $D^0 + \overline{D}^0$ mesons in bins of (p_{T}, y). The first uncertainty is statistical, and the second is the total systematic.

p_{T} [GeV/c]	y				
	$[2.0, 2.5]$	$[2.5, 3.0]$	$[3.0, 3.5]$	$[3.5, 4.0]$	$[4.0, 4.5]$
$[0, 1]$	$1.49^{+0.03}_{-0.03}{}^{+0.23}_{-0.20}$	$1.61^{+0.01}_{-0.01}{}^{+0.13}_{-0.15}$	$1.72^{+0.02}_{-0.02}{}^{+0.13}_{-0.10}$	$1.88^{+0.02}_{-0.02}{}^{+0.12}_{-0.11}$	$2.12^{+0.06}_{-0.05}{}^{+0.20}_{-0.19}$
$[1, 2]$	$1.61^{+0.02}_{-0.02}{}^{+0.20}_{-0.18}$	$1.72^{+0.01}_{-0.01}{}^{+0.13}_{-0.12}$	$1.88^{+0.01}_{-0.01}{}^{+0.12}_{-0.10}$	$2.04^{+0.02}_{-0.02}{}^{+0.12}_{-0.11}$	$2.31^{+0.04}_{-0.04}{}^{+0.17}_{-0.14}$
$[2, 3]$	$1.78^{+0.02}_{-0.02}{}^{+0.15}_{-0.17}$	$1.94^{+0.01}_{-0.01}{}^{+0.14}_{-0.10}$	$2.20^{+0.02}_{-0.02}{}^{+0.13}_{-0.11}$	$2.35^{+0.02}_{-0.02}{}^{+0.15}_{-0.12}$	$2.70^{+0.05}_{-0.05}{}^{+0.17}_{-0.17}$
$[3, 4]$	$2.03^{+0.02}_{-0.02}{}^{+0.14}_{-0.16}$	$2.20^{+0.02}_{-0.02}{}^{+0.14}_{-0.11}$	$2.35^{+0.02}_{-0.02}{}^{+0.14}_{-0.12}$	$2.69^{+0.03}_{-0.03}{}^{+0.19}_{-0.16}$	$3.33^{+0.09}_{-0.09}{}^{+0.32}_{-0.31}$
$[4, 5]$	$2.19^{+0.03}_{-0.03}{}^{+0.17}_{-0.13}$	$2.48^{+0.03}_{-0.02}{}^{+0.16}_{-0.12}$	$2.65^{+0.03}_{-0.03}{}^{+0.16}_{-0.14}$	$3.07^{+0.05}_{-0.05}{}^{+0.17}_{-0.19}$	$3.04^{+0.16}_{-0.15}{}^{+0.63}_{-0.55}$
$[5, 6]$	$2.57^{+0.05}_{-0.04}{}^{+0.21}_{-0.15}$	$2.66^{+0.04}_{-0.04}{}^{+0.17}_{-0.13}$	$2.90^{+0.05}_{-0.04}{}^{+0.16}_{-0.18}$	$3.15^{+0.08}_{-0.08}{}^{+0.22}_{-0.21}$	$5.6^{+1.0}_{-0.7}{}^{+2.2}_{-1.6}$
$[6, 7]$	$2.55^{+0.06}_{-0.05}{}^{+0.19}_{-0.16}$	$2.95^{+0.06}_{-0.06}{}^{+0.19}_{-0.16}$	$3.27^{+0.07}_{-0.07}{}^{+0.18}_{-0.21}$	$3.85^{+0.16}_{-0.15}{}^{+0.44}_{-0.44}$	
$[7, 8]$	$2.67^{+0.08}_{-0.08}{}^{+0.22}_{-0.17}$	$3.00^{+0.08}_{-0.07}{}^{+0.20}_{-0.18}$	$3.44^{+0.11}_{-0.10}{}^{+0.21}_{-0.26}$	$3.93^{+0.32}_{-0.28}{}^{+0.91}_{-0.73}$	

Table 11: The ratios of differential production cross-sections, $R_{13/5}$, for prompt $D^+ + D^-$ mesons in bins of (p_{T}, y). The first uncertainty is statistical, and the second is the total systematic.

	y				
p_{T} [GeV/c]	$[2.0, 2.5]$	$[2.5, 3.0]$	$[3.0, 3.5]$	$[3.5, 4.0]$	$[4.0, 4.5]$
$[0, 1]$		$2.10 \,^{+\,0.23\,+\,0.69}_{-\,0.19\,-\,0.44}$	$1.83 \,^{+\,0.12\,+\,0.32}_{-\,0.11\,-\,0.28}$	$1.66 \,^{+\,0.13\,+\,0.28}_{-\,0.12\,-\,0.25}$	
$[1, 2]$	$1.80 \,^{+\,0.07\,+\,0.44}_{-\,0.07\,-\,0.38}$	$1.69 \,^{+\,0.02\,+\,0.31}_{-\,0.02\,-\,0.20}$	$1.88 \,^{+\,0.02\,+\,0.18}_{-\,0.02\,-\,0.19}$	$2.08 \,^{+\,0.03\,+\,0.17}_{-\,0.03\,-\,0.17}$	$2.25 \,^{+\,0.06\,+\,0.24}_{-\,0.06\,-\,0.22}$
$[2, 3]$	$1.72 \,^{+\,0.03\,+\,0.30}_{-\,0.03\,-\,0.27}$	$1.97 \,^{+\,0.01\,+\,0.25}_{-\,0.01\,-\,0.18}$	$2.09 \,^{+\,0.01\,+\,0.15}_{-\,0.01\,-\,0.17}$	$2.25 \,^{+\,0.02\,+\,0.15}_{-\,0.02\,-\,0.16}$	$2.64 \,^{+\,0.05\,+\,0.22}_{-\,0.04\,-\,0.19}$
$[3, 4]$	$1.87 \,^{+\,0.03\,+\,0.28}_{-\,0.03\,-\,0.26}$	$2.21 \,^{+\,0.02\,+\,0.22}_{-\,0.02\,-\,0.17}$	$2.41 \,^{+\,0.02\,+\,0.18}_{-\,0.02\,-\,0.15}$	$2.60 \,^{+\,0.03\,+\,0.18}_{-\,0.03\,-\,0.15}$	$2.81 \,^{+\,0.06\,+\,0.21}_{-\,0.05\,-\,0.21}$
$[4, 5]$	$2.12 \,^{+\,0.03\,+\,0.27}_{-\,0.03\,-\,0.26}$	$2.48 \,^{+\,0.02\,+\,0.22}_{-\,0.02\,-\,0.17}$	$2.55 \,^{+\,0.03\,+\,0.19}_{-\,0.03\,-\,0.14}$	$2.96 \,^{+\,0.04\,+\,0.21}_{-\,0.04\,-\,0.17}$	$3.59 \,^{+\,0.11\,+\,0.23}_{-\,0.10\,-\,0.29}$
$[5, 6]$	$2.40 \,^{+\,0.04\,+\,0.25}_{-\,0.04\,-\,0.27}$	$2.68 \,^{+\,0.03\,+\,0.22}_{-\,0.03\,-\,0.17}$	$2.95 \,^{+\,0.04\,+\,0.21}_{-\,0.04\,-\,0.16}$	$3.25 \,^{+\,0.06\,+\,0.24}_{-\,0.06\,-\,0.20}$	$4.51 \,^{+\,0.24\,+\,0.47}_{-\,0.22\,-\,0.48}$
$[6, 7]$	$2.54 \,^{+\,0.06\,+\,0.25}_{-\,0.06\,-\,0.25}$	$2.80 \,^{+\,0.05\,+\,0.22}_{-\,0.05\,-\,0.17}$	$3.01 \,^{+\,0.06\,+\,0.22}_{-\,0.06\,-\,0.17}$	$3.92 \,^{+\,0.11\,+\,0.25}_{-\,0.11\,-\,0.29}$	$4.27 \,^{+\,0.48\,+\,0.61}_{-\,0.39\,-\,0.50}$
$[7, 8]$	$2.72 \,^{+\,0.08\,+\,0.28}_{-\,0.07\,-\,0.24}$	$3.10 \,^{+\,0.07\,+\,0.25}_{-\,0.07\,-\,0.19}$	$3.39 \,^{+\,0.09\,+\,0.27}_{-\,0.08\,-\,0.20}$	$3.70 \,^{+\,0.16\,+\,0.29}_{-\,0.14\,-\,0.34}$	

Table 12: The ratios of differential production cross-sections, $R_{13/5}$, for prompt $D_s^+ + D_s^-$ mesons in bins of (p_{T}, y). The first uncertainty is statistical, and the second is the total systematic.

	y				
p_{T} [GeV/c]	$[2.0, 2.5]$	$[2.5, 3.0]$	$[3.0, 3.5]$	$[3.5, 4.0]$	$[4.0, 4.5]$
$[1, 2]$	$1.30 \,^{+\,0.28\,+\,0.54}_{-\,0.21\,-\,0.37}$	$1.48 \,^{+\,0.12\,+\,0.42}_{-\,0.10\,-\,0.24}$	$1.83 \,^{+\,0.14\,+\,0.26}_{-\,0.12\,-\,0.24}$	$2.30 \,^{+\,0.26\,+\,0.41}_{-\,0.22\,-\,0.31}$	
$[2, 3]$	$1.58 \,^{+\,0.10\,+\,0.41}_{-\,0.09\,-\,0.32}$	$1.76 \,^{+\,0.05\,+\,0.24}_{-\,0.05\,-\,0.17}$	$2.10 \,^{+\,0.07\,+\,0.19}_{-\,0.06\,-\,0.17}$	$2.77 \,^{+\,0.13\,+\,0.22}_{-\,0.13\,-\,0.22}$	$2.71 \,^{+\,0.36\,+\,0.45}_{-\,0.28\,-\,0.38}$
$[3, 4]$	$1.94 \,^{+\,0.10\,+\,0.35}_{-\,0.09\,-\,0.30}$	$2.06 \,^{+\,0.06\,+\,0.21}_{-\,0.06\,-\,0.19}$	$2.44 \,^{+\,0.08\,+\,0.20}_{-\,0.08\,-\,0.16}$	$2.58 \,^{+\,0.12\,+\,0.20}_{-\,0.11\,-\,0.18}$	$2.75 \,^{+\,0.30\,+\,0.32}_{-\,0.25\,-\,0.27}$
$[4, 5]$	$2.09 \,^{+\,0.12\,+\,0.33}_{-\,0.11\,-\,0.26}$	$2.35 \,^{+\,0.09\,+\,0.23}_{-\,0.08\,-\,0.17}$	$2.38 \,^{+\,0.10\,+\,0.18}_{-\,0.09\,-\,0.15}$	$3.42 \,^{+\,0.21\,+\,0.25}_{-\,0.19\,-\,0.26}$	$3.28 \,^{+\,0.48\,+\,0.41}_{-\,0.38\,-\,0.33}$
$[5, 6]$	$2.82 \,^{+\,0.20\,+\,0.35}_{-\,0.18\,-\,0.33}$	$3.26 \,^{+\,0.18\,+\,0.33}_{-\,0.16\,-\,0.20}$	$2.56 \,^{+\,0.14\,+\,0.20}_{-\,0.13\,-\,0.18}$	$3.39 \,^{+\,0.29\,+\,0.38}_{-\,0.25\,-\,0.26}$	$4.0 \,^{+\,\,1.0\,+\,\,0.7}_{-\,\,0.7\,-\,\,0.6}$
$[6, 7]$	$2.60 \,^{+\,0.23\,+\,0.32}_{-\,0.19\,-\,0.28}$	$2.94 \,^{+\,0.20\,+\,0.28}_{-\,0.18\,-\,0.22}$	$3.59 \,^{+\,0.30\,+\,0.29}_{-\,0.26\,-\,0.28}$	$3.58 \,^{+\,0.47\,+\,0.49}_{-\,0.37\,-\,0.34}$	
$[7, 8]$	$2.50 \,^{+\,0.27\,+\,0.37}_{-\,0.22\,-\,0.22}$	$2.79 \,^{+\,0.26\,+\,0.24}_{-\,0.22\,-\,0.25}$	$3.47 \,^{+\,0.38\,+\,0.37}_{-\,0.32\,-\,0.29}$	$4.12 \,^{+\,0.72\,+\,0.76}_{-\,0.55\,-\,0.56}$	

Table 13: The ratios of differential production cross-sections, $R_{13/5}$, for prompt $D^{*+} + D^{*-}$ mesons in bins of (p_{T}, y). The first uncertainty is statistical, and the second is the total systematic.

	y				
p_{T} [GeV/c]	$[2.0, 2.5]$	$[2.5, 3.0]$	$[3.0, 3.5]$	$[3.5, 4.0]$	$[4.0, 4.5]$
$[1, 2]$		$1.33 \pm 0.07 \pm 0.15$	$1.70 \pm 0.04 \pm 0.19$	$1.81 \pm 0.06 \pm 0.21$	$2.52 \pm 0.17 \pm 0.40$
$[2, 3]$	$1.51 \pm 0.18 \pm 0.32$	$1.70 \pm 0.04 \pm 0.20$	$2.01 \pm 0.04 \pm 0.21$	$2.29 \pm 0.06 \pm 0.27$	$2.47 \pm 0.13 \pm 0.33$
$[3, 4]$	$1.60 \pm 0.09 \pm 0.20$	$1.99 \pm 0.04 \pm 0.18$	$2.08 \pm 0.04 \pm 0.21$	$2.49 \pm 0.07 \pm 0.28$	$3.00 \pm 0.20 \pm 0.35$
$[4, 5]$	$1.82 \pm 0.09 \pm 0.21$	$2.18 \pm 0.05 \pm 0.20$	$2.25 \pm 0.05 \pm 0.20$	$2.54 \pm 0.09 \pm 0.30$	$3.24 \pm 0.42 \pm 0.77$
$[5, 6]$	$1.96 \pm 0.10 \pm 0.21$	$2.43 \pm 0.08 \pm 0.22$	$2.72 \pm 0.09 \pm 0.25$	$3.22 \pm 0.17 \pm 0.33$	$2.61 \pm 0.16 \pm 0.65$
$[6, 7]$	$2.07 \pm 0.13 \pm 0.22$	$2.72 \pm 0.11 \pm 0.25$	$2.95 \pm 0.13 \pm 0.26$	$3.10 \pm 0.25 \pm 0.32$	
$[7, 8]$	$2.67 \pm 0.20 \pm 0.30$	$2.71 \pm 0.14 \pm 0.27$	$3.23 \pm 0.20 \pm 0.31$	$3.89 \pm 0.53 \pm 0.61$	

C Cross-section ratios for different mesons

The numerical values of the cross-section ratios between mesons, described in Sec. 5, are given in (p_{T}, y) bins in Tables 14–19.

Table 14: The ratios of the measurements of cross-section times branching fraction for prompt D^+ and D^0 mesons in bins of (p_{T}, y). The first uncertainty is statistical, and the second is the total systematic. All values are given in percent.

p_{T} [GeV/c]	y			
	$[2.0, 2.5]$	$[2.5, 3.0]$	$[3.0, 3.5]$	$[3.5, 4.0]$	$[4.0, 4.5]$
$[0, 1]$		$101 \pm {}^{9}_{9} \pm {}^{12}_{14}$	$83.9 \pm {}^{5.0}_{5.0} \pm {}^{8.4}_{6.6}$	$101.0 \pm {}^{7.2}_{7.1} \pm {}^{9.9}_{8.9}$	
$[1, 2]$	$84 \pm {}^{3}_{3} \pm {}^{11}_{10}$	$88.2 \pm {}^{1.1}_{1.1} \pm {}^{3.6}_{4.1}$	$94.9 \pm {}^{1.0}_{1.0} \pm {}^{5.4}_{3.2}$	$89.4 \pm {}^{1.2}_{1.2} \pm {}^{4.2}_{3.0}$	$98.1 \pm {}^{2.9}_{2.8} \pm {}^{7.2}_{6.3}$
$[2, 3]$	$91.9 \pm {}^{1.7}_{1.6} \pm {}^{7.3}_{6.7}$	$94.0 \pm {}^{0.8}_{0.8} \pm {}^{2.8}_{3.7}$	$98.7 \pm {}^{0.9}_{0.9} \pm {}^{3.9}_{2.8}$	$95.9 \pm {}^{1.1}_{1.1} \pm {}^{4.0}_{3.1}$	$99.4 \pm {}^{2.4}_{2.3} \pm {}^{5.2}_{5.1}$
$[3, 4]$	$98.8 \pm {}^{1.7}_{1.7} \pm {}^{4.8}_{5.8}$	$99.0 \pm {}^{1.0}_{1.0} \pm {}^{2.0}_{3.9}$	$101.0 \pm {}^{1.1}_{1.1} \pm {}^{2.9}_{3.5}$	$99.0 \pm {}^{1.4}_{1.4} \pm {}^{3.4}_{3.9}$	$111.8 \pm {}^{3.6}_{3.6} \pm {}^{8.1}_{8.1}$
$[4, 5]$	$106.2 \pm {}^{2.0}_{2.0} \pm {}^{4.4}_{5.2}$	$103.1 \pm {}^{1.4}_{1.4} \pm {}^{2.5}_{3.7}$	$104.9 \pm {}^{1.5}_{1.5} \pm {}^{3.3}_{3.8}$	$102.6 \pm {}^{2.1}_{2.0} \pm {}^{3.4}_{3.8}$	$106 \pm {}^{6}_{6} \pm {}^{16}_{15}$
$[5, 6]$	$107.2 \pm {}^{2.6}_{2.5} \pm {}^{4.4}_{4.7}$	$107.5 \pm {}^{1.9}_{1.9} \pm {}^{3.5}_{3.9}$	$104.1 \pm {}^{2.1}_{2.1} \pm {}^{3.3}_{4.2}$	$103.2 \pm {}^{3.1}_{3.0} \pm {}^{5.1}_{5.7}$	$184 \pm {}^{32}_{24} \pm {}^{58}_{44}$
$[6, 7]$	$106.6 \pm {}^{3.2}_{3.1} \pm {}^{4.5}_{5.1}$	$106.7 \pm {}^{2.6}_{2.5} \pm {}^{3.8}_{4.3}$	$111.8 \pm {}^{3.1}_{3.0} \pm {}^{4.3}_{5.0}$	$110.7 \pm {}^{5.4}_{5.0} \pm {}^{9.7}_{9.8}$	
$[7, 8]$	$113.6 \pm {}^{4.4}_{4.2} \pm {}^{5.5}_{6.4}$	$99.4 \pm {}^{3.3}_{3.0} \pm {}^{3.4}_{5.1}$	$106.4 \pm {}^{4.1}_{3.9} \pm {}^{5.2}_{6.1}$	$130 \pm {}^{11}_{10} \pm {}^{24}_{21}$	
$[8, 9]$	$108.4 \pm {}^{5.4}_{5.1} \pm {}^{6.4}_{6.9}$	$106.4 \pm {}^{4.7}_{4.3} \pm {}^{4.9}_{6.8}$	$102.7 \pm {}^{5.7}_{5.5} \pm {}^{8.2}_{7.9}$	$202 \pm {}^{35}_{28} \pm {}^{53}_{37}$	
$[9, 10]$	$91.3 \pm {}^{5.6}_{5.4} \pm {}^{7.0}_{6.6}$	$101.9 \pm {}^{5.8}_{5.5} \pm {}^{6.3}_{7.7}$	$125 \pm {}^{10}_{9} \pm {}^{17}_{15}$		

Table 15: The ratios of the measurements of cross-section times branching fraction for prompt D_s^+ and D^0 mesons in bins of (p_{T}, y). The first uncertainty is statistical, and the second is the total systematic. All values are given in percent.

	y				
p_{T} [GeV/c]	$[2.0, 2.5]$	$[2.5, 3.0]$	$[3.0, 3.5]$	$[3.5, 4.0]$	$[4.0, 4.5]$
$[1, 2]$	$6.8^{+\ 1.0\ +\ 1.5}_{-\ 1.0\ -\ 1.1}$	$9.56^{+\ 0.57\ +\ 0.54}_{-\ 0.58\ -\ 0.60}$	$9.37^{+\ 0.58\ +\ 0.72}_{-\ 0.59\ -\ 0.52}$	$7.91^{+\ 0.72\ +\ 0.66}_{-\ 0.73\ -\ 0.49}$	
$[2, 3]$	$10.7^{+\ 0.6\ +\ 1.7}_{-\ 0.6\ -\ 1.3}$	$11.31^{+\ 0.32\ +\ 0.38}_{-\ 0.32\ -\ 0.47}$	$11.39^{+\ 0.34\ +\ 0.52}_{-\ 0.35\ -\ 0.40}$	$9.17^{+\ 0.41\ +\ 0.48}_{-\ 0.41\ -\ 0.35}$	$9.1^{+\ 1.0\ +\ 1.2}_{-\ 1.0\ -\ 0.9}$
$[3, 4]$	$10.80^{+\ 0.52\ +\ 0.98}_{-\ 0.53\ -\ 0.79}$	$11.76^{+\ 0.35\ +\ 0.30}_{-\ 0.34\ -\ 0.45}$	$11.10^{+\ 0.36\ +\ 0.43}_{-\ 0.36\ -\ 0.33}$	$11.53^{+\ 0.50\ +\ 0.52}_{-\ 0.52\ -\ 0.45}$	$12.0^{+\ 1.2\ +\ 1.0}_{-\ 1.2\ -\ 1.0}$
$[4, 5]$	$11.30^{+\ 0.59\ +\ 0.67}_{-\ 0.58\ -\ 0.77}$	$12.67^{+\ 0.45\ +\ 0.32}_{-\ 0.46\ -\ 0.51}$	$12.70^{+\ 0.52\ +\ 0.49}_{-\ 0.52\ -\ 0.45}$	$10.84^{+\ 0.62\ +\ 0.51}_{-\ 0.62\ -\ 0.40}$	$13.0^{+\ 1.7\ +\ 2.3}_{-\ 1.7\ -\ 2.0}$
$[5, 6]$	$11.41^{+\ 0.75\ +\ 0.63}_{-\ 0.75\ -\ 0.65}$	$10.62^{+\ 0.55\ +\ 0.39}_{-\ 0.53\ -\ 0.41}$	$14.23^{+\ 0.75\ +\ 0.61}_{-\ 0.72\ -\ 0.62}$	$11.88^{+\ 0.96\ +\ 0.72}_{-\ 0.94\ -\ 0.76}$	$23.1^{+\ 6.3\ +\ 7.6}_{-\ 5.2\ -\ 5.7}$
$[6, 7]$	$11.75^{+\ 0.92\ +\ 0.70}_{-\ 0.94\ -\ 0.75}$	$12.98^{+\ 0.86\ +\ 0.71}_{-\ 0.82\ -\ 0.54}$	$11.05^{+\ 0.85\ +\ 0.59}_{-\ 0.85\ -\ 0.52}$	$12.8^{+\ 1.5\ +\ 1.5}_{-\ 1.5\ -\ 1.3}$	
$[7, 8]$	$14.7^{+\ 1.4\ +\ 0.9}_{-\ 1.4\ -\ 1.2}$	$11.47^{+\ 0.97\ +\ 0.78}_{-\ 0.97\ -\ 0.56}$	$11.6^{+\ 1.2\ +\ 0.8}_{-\ 1.2\ -\ 0.8}$	$14.8^{+\ 2.5\ +\ 3.5}_{-\ 2.3\ -\ 2.6}$	
$[8, 9]$	$9.8^{+\ 1.4\ +\ 0.8}_{-\ 1.4\ -\ 0.7}$	$10.5^{+\ 1.2\ +\ 0.8}_{-\ 1.2\ -\ 0.7}$	$11.6^{+\ 1.6\ +\ 1.3}_{-\ 1.5\ -\ 1.1}$		
$[9, 10]$	$11.4^{+\ 1.8\ +\ 1.3}_{-\ 1.8\ -\ 1.2}$	$12.5^{+\ 1.8\ +\ 1.3}_{-\ 1.7\ -\ 1.0}$	$15.2^{+\ 2.9\ +\ 2.7}_{-\ 2.7\ -\ 2.1}$		

Table 16: The ratios of the measurements of cross-section times branching fraction for prompt D^{*+} and D^0 mesons in bins of (p_{T}, y). The first uncertainty is statistical, and the second is the total systematic. All values are given in percent.

	y				
p_{T} [GeV/c]	$[2.0, 2.5]$	$[2.5, 3.0]$	$[3.0, 3.5]$	$[3.5, 4.0]$	$[4.0, 4.5]$
$[1, 2]$		$28.6 \pm 1.3 \pm 2.1 \pm 1.2$	$26.9 \pm 0.6 \pm 1.5 \pm 1.7$	$25.2 \pm 0.7 \pm 1.5 \pm 1.7$	$23.4 \pm 1.4 \pm 1.6 \pm 1.9$
$[2, 3]$	$31.7 \pm 3.2 \pm 3.0 \pm 3.2$	$30.5 \pm 0.7 \pm 1.1 \pm 1.2$	$29.8 \pm 0.5 \pm 1.5 \pm 1.9$	$26.5 \pm 0.7 \pm 1.5 \pm 1.8$	$28.3 \pm 1.5 \pm 2.9 \pm 2.7$
$[3, 4]$	$35.4 \pm 1.8 \pm 1.5 \pm 2.1$	$31.9 \pm 0.7 \pm 1.3 \pm 1.1$	$32.4 \pm 0.7 \pm 1.9 \pm 1.7$	$28.2 \pm 0.8 \pm 1.6 \pm 1.9$	$29.7 \pm 2.0 \pm 2.1 \pm 2.5$
$[4, 5]$	$34.5 \pm 1.6 \pm 1.6 \pm 1.7$	$33.2 \pm 0.8 \pm 1.2 \pm 1.4$	$33.6 \pm 0.9 \pm 2.0 \pm 1.6$	$34.1 \pm 1.2 \pm 2.4 \pm 2.6$	$28.4 \pm 3.5 \pm 7.5 \pm 5.5$
$[5, 6]$	$35.8 \pm 1.8 \pm 1.8 \pm 1.9$	$32.2 \pm 1.0 \pm 1.4 \pm 1.4$	$31.9 \pm 1.1 \pm 1.8 \pm 1.7$	$31.4 \pm 1.7 \pm 2.3 \pm 2.0$	$67 \pm 11 \pm 23 \pm 17$
$[6, 7]$	$38.1 \pm 2.2 \pm 2.0 \pm 2.2$	$33.4 \pm 1.4 \pm 1.5 \pm 1.6$	$32.9 \pm 1.6 \pm 1.8 \pm 1.8$	$36.6 \pm 3.0 \pm 3.5 \pm 3.7$	
$[7, 8]$	$33.2 \pm 2.4 \pm 2.0 \pm 2.2$	$32.9 \pm 1.8 \pm 1.5 \pm 2.0$	$33.9 \pm 2.2 \pm 2.3 \pm 2.2$	$37.2 \pm 5.2 \pm 7.1 \pm 6.3$	
$[8, 9]$	$29.9 \pm 2.8 \pm 2.2 \pm 2.4$	$34.2 \pm 2.5 \pm 1.9 \pm 2.4$	$33.2 \pm 3.0 \pm 3.2 \pm 2.8$	$59 \pm 14 \pm 24 \pm 13$	
$[9, 10]$	$35.8 \pm 3.9 \pm 3.1 \pm 3.0$	$33.8 \pm 3.1 \pm 2.3 \pm 2.9$	$57.2 \pm 6.5 \pm 9.6 \pm 8.1$		

Table 17: The ratios of the measurements of cross-section times branching fraction for prompt D_s^+ and D^+ mesons in bins of (p_{T}, y). The first uncertainty is statistical, and the second is the total systematic. All values are given in percent.

	y				
p_{T} [GeV/c]	$[2.0, 2.5]$	$[2.5, 3.0]$	$[3.0, 3.5]$	$[3.5, 4.0]$	$[4.0, 4.5]$
$[1, 2]$	$8.0^{+\ 1.3\ +\ 2.1}_{-\ 1.2\ -\ 1.5}$	$10.84^{+\ 0.67\ +\ 0.55}_{-\ 0.66\ -\ 0.54}$	$9.87^{+\ 0.62\ +\ 0.47}_{-\ 0.63\ -\ 0.55}$	$8.84^{+\ 0.82\ +\ 0.60}_{-\ 0.82\ -\ 0.58}$	
$[2, 3]$	$11.7^{+\ 0.7\ +\ 1.9}_{-\ 0.6\ -\ 1.5}$	$12.03^{+\ 0.33\ +\ 0.34}_{-\ 0.34\ -\ 0.28}$	$11.53^{+\ 0.35\ +\ 0.33}_{-\ 0.34\ -\ 0.35}$	$9.56^{+\ 0.42\ +\ 0.38}_{-\ 0.42\ -\ 0.38}$	$9.2^{+\ 1.0\ +\ 1.3}_{-\ 1.0\ -\ 0.9}$
$[3, 4]$	$10.9^{+\ 0.5\ +\ 1.1}_{-\ 0.5\ -\ 0.8}$	$11.87^{+\ 0.35\ +\ 0.36}_{-\ 0.34\ -\ 0.17}$	$10.99^{+\ 0.36\ +\ 0.40}_{-\ 0.36\ -\ 0.21}$	$11.63^{+\ 0.51\ +\ 0.54}_{-\ 0.51\ -\ 0.33}$	$10.7^{+\ 1.0\ +\ 0.9}_{-\ 1.0\ -\ 0.8}$
$[4, 5]$	$10.64^{+\ 0.56\ +\ 0.68}_{-\ 0.56\ -\ 0.64}$	$12.29^{+\ 0.45\ +\ 0.34}_{-\ 0.44\ -\ 0.33}$	$12.11^{+\ 0.49\ +\ 0.47}_{-\ 0.50\ -\ 0.35}$	$10.57^{+\ 0.61\ +\ 0.52}_{-\ 0.60\ -\ 0.36}$	$12.3^{+\ 1.6\ +\ 1.1}_{-\ 1.6\ -\ 0.9}$
$[5, 6]$	$10.64^{+\ 0.72\ +\ 0.54}_{-\ 0.71\ -\ 0.53}$	$9.88^{+\ 0.51\ +\ 0.38}_{-\ 0.50\ -\ 0.28}$	$13.68^{+\ 0.70\ +\ 0.61}_{-\ 0.69\ -\ 0.45}$	$11.52^{+\ 0.91\ +\ 0.71}_{-\ 0.90\ -\ 0.56}$	$12.6^{+\ 2.6\ +\ 1.7}_{-\ 2.6\ -\ 1.3}$
$[6, 7]$	$11.01^{+\ 0.89\ +\ 0.64}_{-\ 0.87\ -\ 0.57}$	$12.17^{+\ 0.79\ +\ 0.64}_{-\ 0.77\ -\ 0.37}$	$9.87^{+\ 0.75\ +\ 0.63}_{-\ 0.74\ -\ 0.40}$	$11.5^{+\ 1.3\ +\ 1.1}_{-\ 1.3\ -\ 0.8}$	
$[7, 8]$	$13.0^{+\ 1.2\ +\ 0.9}_{-\ 1.2\ -\ 0.9}$	$11.53^{+\ 0.97\ +\ 0.88}_{-\ 0.97\ -\ 0.39}$	$10.9^{+\ 1.1\ +\ 0.8}_{-\ 1.1\ -\ 0.5}$	$11.4^{+\ 1.7\ +\ 1.8}_{-\ 1.7\ -\ 1.3}$	
$[8, 9]$	$9.1^{+\ 1.3\ +\ 0.8}_{-\ 1.3\ -\ 0.6}$	$9.9^{+\ 1.2\ +\ 0.9}_{-\ 1.1\ -\ 0.4}$	$11.4^{+\ 1.5\ +\ 1.1}_{-\ 1.5\ -\ 0.9}$		
$[9, 10]$	$12.5^{+\ 1.9\ +\ 1.4}_{-\ 1.9\ -\ 1.1}$	$12.3^{+\ 1.7\ +\ 1.4}_{-\ 1.7\ -\ 0.7}$	$12.2^{+\ 2.2\ +\ 1.5}_{-\ 2.1\ -\ 1.3}$		

Table 18: The ratios of the measurements of cross-section times branching fraction for prompt D^{*+} and D^+ mesons in bins of (p_{T}, y). The first uncertainty is statistical, and the second is the total systematic. All values are given in percent.

	y				
p_{T} [GeV/c]	$[2.0, 2.5]$	$[2.5, 3.0]$	$[3.0, 3.5]$	$[3.5, 4.0]$	$[4.0, 4.5]$
$[1, 2]$		$32.5 \,^{+\,1.5\,+\,2.2}_{-\,1.5\,-\,0.8}$	$28.4 \,^{+\,0.7\,+\,0.5}_{-\,0.7\,-\,1.6}$	$28.2 \,^{+\,0.9\,+\,0.9}_{-\,0.9\,-\,1.6}$	$23.9 \,^{+\,1.6\,+\,1.6}_{-\,1.5\,-\,2.0}$
$[2, 3]$	$34.5 \,^{+\,3.4\,+\,3.8}_{-\,3.5\,-\,3.9}$	$32.4 \,^{+\,0.8\,+\,1.1}_{-\,0.8\,-\,0.9}$	$30.2 \,^{+\,0.5\,+\,0.8}_{-\,0.5\,-\,1.5}$	$27.6 \,^{+\,0.7\,+\,0.9}_{-\,0.7\,-\,1.5}$	$28.5 \,^{+\,1.5\,+\,2.8}_{-\,1.4\,-\,2.5}$
$[3, 4]$	$35.8 \,^{+\,1.8\,+\,2.2}_{-\,1.8\,-\,2.2}$	$32.2 \,^{+\,0.7\,+\,1.4}_{-\,0.7\,-\,0.4}$	$32.1 \,^{+\,0.6\,+\,1.6}_{-\,0.6\,-\,1.2}$	$28.5 \,^{+\,0.8\,+\,1.4}_{-\,0.8\,-\,1.5}$	$26.5 \,^{+\,1.7\,+\,1.4}_{-\,1.7\,-\,1.7}$
$[4, 5]$	$32.5 \,^{+\,1.5\,+\,1.7}_{-\,1.5\,-\,1.4}$	$32.2 \,^{+\,0.8\,+\,1.1}_{-\,0.8\,-\,0.9}$	$32.0 \,^{+\,0.8\,+\,1.7}_{-\,0.8\,-\,1.1}$	$33.2 \,^{+\,1.1\,+\,2.2}_{-\,1.1\,-\,2.2}$	$26.9 \,^{+\,3.1\,+\,5.8}_{-\,3.1\,-\,4.0}$
$[5, 6]$	$33.4 \,^{+\,1.7\,+\,1.5}_{-\,1.7\,-\,1.5}$	$29.9 \,^{+\,1.0\,+\,1.1}_{-\,0.9\,-\,1.0}$	$30.6 \,^{+\,1.1\,+\,1.6}_{-\,1.1\,-\,1.2}$	$30.5 \,^{+\,1.6\,+\,1.9}_{-\,1.6\,-\,1.3}$	$36.6 \,^{+\,2.2\,+\,5.8}_{-\,2.0\,-\,4.7}$
$[6, 7]$	$35.8 \,^{+\,2.1\,+\,1.8}_{-\,2.1\,-\,1.7}$	$31.3 \,^{+\,1.3\,+\,1.2}_{-\,1.2\,-\,1.2}$	$29.4 \,^{+\,1.4\,+\,1.6}_{-\,1.4\,-\,1.3}$	$33.1 \,^{+\,2.6\,+\,2.1}_{-\,2.5\,-\,2.1}$	
$[7, 8]$	$29.2 \,^{+\,2.1\,+\,1.8}_{-\,2.1\,-\,1.6}$	$33.1 \,^{+\,1.7\,+\,1.6}_{-\,1.7\,-\,1.4}$	$31.8 \,^{+\,2.0\,+\,2.0}_{-\,1.9\,-\,1.5}$	$28.6 \,^{+\,3.6\,+\,3.1}_{-\,3.5\,-\,3.0}$	
$[8, 9]$	$27.6 \,^{+\,2.5\,+\,1.9}_{-\,2.5\,-\,1.8}$	$32.2 \,^{+\,2.2\,+\,1.9}_{-\,2.2\,-\,1.6}$	$32.3 \,^{+\,2.7\,+\,2.5}_{-\,2.6\,-\,2.1}$	$29.0 \,^{+\,5.4\,+\,8.8}_{-\,5.3\,-\,5.6}$	
$[9, 10]$	$39.3 \,^{+\,4.2\,+\,3.2}_{-\,4.1\,-\,2.9}$	$33.2 \,^{+\,3.0\,+\,2.4}_{-\,2.9\,-\,2.2}$	$45.8 \,^{+\,4.8\,+\,5.8}_{-\,4.6\,-\,5.1}$		

Table 19: The ratios of the measurements of cross-section times branching fraction for prompt D_s^+ and D^{*+} mesons in bins of (p_{T}, y). The first uncertainty is statistical, and the second is the total systematic. All values are given in percent.

	y				
p_{T} [GeV/c]	$[2.0, 2.5]$	$[2.5, 3.0]$	$[3.0, 3.5]$	$[3.5, 4.0]$	$[4.0, 4.5]$
$[1, 2]$		$33.4 \,^{+\,2.6\,+\,1.3}_{-\,2.4\,-\,2.6}$	$34.8 \,^{+\,2.3\,+\,2.7}_{-\,2.3\,-\,1.2}$	$31.4 \,^{+\,3.0\,+\,3.3}_{-\,3.0\,-\,1.9}$	
$[2, 3]$	$33.8 \,^{+\,4.2\,+\,7.2}_{-\,3.5\,-\,4.6}$	$37.0 \,^{+\,1.4\,+\,1.3}_{-\,1.3\,-\,1.3}$	$38.2 \,^{+\,1.3\,+\,2.3}_{-\,1.3\,-\,1.0}$	$34.6 \,^{+\,1.7\,+\,2.7}_{-\,1.7\,-\,1.6}$	$32.1 \,^{+\,3.9\,+\,5.5}_{-\,3.8\,-\,4.0}$
$[3, 4]$	$30.5 \,^{+\,2.2\,+\,3.3}_{-\,2.1\,-\,2.1}$	$36.9 \,^{+\,1.3\,+\,0.8}_{-\,1.3\,-\,1.4}$	$34.3 \,^{+\,1.3\,+\,1.7}_{-\,1.2\,-\,1.6}$	$40.8 \,^{+\,2.1\,+\,3.2}_{-\,2.0\,-\,2.1}$	$40.4 \,^{+\,4.6\,+\,4.2}_{-\,4.5\,-\,2.6}$
$[4, 5]$	$32.8 \,^{+\,2.3\,+\,2.1}_{-\,2.1\,-\,2.1}$	$38.2 \,^{+\,1.6\,+\,1.3}_{-\,1.6\,-\,1.4}$	$37.9 \,^{+\,1.7\,+\,1.8}_{-\,1.7\,-\,2.2}$	$31.9 \,^{+\,2.0\,+\,2.9}_{-\,2.0\,-\,2.1}$	$45.7 \,^{+\,8.3\,+\,9.5}_{-\,7.1\,-\,7.7}$
$[5, 6]$	$31.9 \,^{+\,2.7\,+\,1.9}_{-\,2.5\,-\,1.7}$	$33.0 \,^{+\,1.9\,+\,1.4}_{-\,1.8\,-\,1.2}$	$44.6 \,^{+\,2.7\,+\,2.6}_{-\,2.5\,-\,2.4}$	$37.8 \,^{+\,3.5\,+\,2.6}_{-\,3.3\,-\,2.7}$	$34.3 \,^{+\,6.9\,+\,6.3}_{-\,6.8\,-\,4.9}$
$[6, 7]$	$30.8 \,^{+\,3.0\,+\,2.0}_{-\,2.8\,-\,1.8}$	$38.9 \,^{+\,2.8\,+\,2.5}_{-\,2.8\,-\,1.5}$	$33.6 \,^{+\,2.9\,+\,2.4}_{-\,2.8\,-\,1.9}$	$34.8 \,^{+\,4.8\,+\,3.9}_{-\,4.4\,-\,2.6}$	
$[7, 8]$	$44.5 \,^{+\,5.2\,+\,3.5}_{-\,5.0\,-\,3.0}$	$34.9 \,^{+\,3.3\,+\,3.0}_{-\,3.3\,-\,1.4}$	$34.3 \,^{+\,4.0\,+\,2.9}_{-\,3.7\,-\,2.3}$	$40.0 \,^{+\,8.1\,+\,7.6}_{-\,7.1\,-\,4.8}$	
$[8, 9]$	$32.9 \,^{+\,5.5\,+\,3.3}_{-\,5.2\,-\,2.7}$	$30.6 \,^{+\,4.1\,+\,3.1}_{-\,3.9\,-\,1.5}$	$35.1 \,^{+\,5.4\,+\,3.8}_{-\,5.2\,-\,3.0}$		
$[9, 10]$	$31.9 \,^{+\,6.0\,+\,4.3}_{-\,5.4\,-\,3.3}$	$37.0 \,^{+\,6.0\,+\,4.8}_{-\,5.5\,-\,2.6}$	$26.6 \,^{+\,5.5\,+\,4.3}_{-\,4.9\,-\,3.2}$		

References

[1] R. Gauld, J. Rojo, L. Rottoli, and J. Talbert, *Charm production in the forward region: constraints on the small-x gluon and backgrounds for neutrino astronomy*, JHEP **11** (2015) 009, arXiv:1506.08025.

[2] M. Cacciari, M. L. Mangano, and P. Nason, *Gluon PDF constraints from the ratio of forward heavy-quark production at the LHC at $\sqrt{s} = 7$ and 13 TeV*, Eur. Phys. J. **C75** (2015) 610, arXiv:1507.06197.

[3] B. A. Kniehl, G. Kramer, I. Schienbein, and H. Spiesberger, *Inclusive charmed-meson production at the CERN LHC*, Eur. Phys. J. **C72** (2012) 2082, arXiv:1202.0439.

[4] R. Maciula and A. Szczurek, *Open charm production at the LHC - k_t-factorization approach*, Phys. Rev. **D87** (2013), no. 9 094022, arXiv:1301.3033.

[5] B. A. Kniehl, G. Kramer, I. Schienbein, and H. Spiesberger, *Inclusive $D^{*\pm}$ production in $p\bar{p}$ collisions with massive charm quarks*, Phys. Rev. **D71** (2005) 014018, arXiv:hep-ph/0410289.

[6] B. A. Kniehl and G. Kramer, *D^0, D^+, D_s^+, and Λ_c^+ fragmentation functions from CERN LEP1*, Phys. Rev. **D71** (2005) 094013, arXiv:hep-ph/0504058.

[7] B. A. Kniehl, G. Kramer, I. Schienbein, and H. Spiesberger, *Reconciling open charm production at the Fermilab Tevatron with QCD*, Phys. Rev. Lett. **96** (2006) 012001, arXiv:hep-ph/0508129.

[8] T. Kneesch, B. A. Kniehl, G. Kramer, and I. Schienbein, *Charmed-meson fragmentation functions with finite-mass corrections*, Nucl. Phys. **B799** (2008) 34, arXiv:0712.0481.

[9] B. A. Kniehl, G. Kramer, I. Schienbein, and H. Spiesberger, *Open charm hadroproduction and the charm content of the proton*, Phys. Rev. **D79** (2009) 094009, arXiv:0901.4130.

[10] M. Cacciari, M. Greco, and P. Nason, *The p_{T} spectrum in heavy flavor hadroproduction*, JHEP **05** (1998) 007, arXiv:hep-ph/9803400.

[11] M. Cacciari and P. Nason, *Charm cross-sections for the Tevatron Run II*, JHEP **09** (2003) 006, arXiv:hep-ph/0306212.

[12] M. Cacciari, P. Nason, and C. Oleari, *A Study of heavy flavored meson fragmentation functions in e^+ e^- annihilation*, JHEP **04** (2006) 006, arXiv:hep-ph/0510032.

[13] M. Cacciari *et al.*, *Theoretical predictions for charm and bottom production at the LHC*, JHEP **10** (2012) 137, arXiv:1205.6344.

[14] PROSA Collaboration, O. Zenaiev *et al.*, *Impact of heavy-flavour production cross sections measured by the LHCb experiment on parton distribution functions at low x*, Eur. Phys. J. **C75** (2015) 396, arXiv:1503.04581.

[15] CDF collaboration, D. Acosta *et al.*, *Measurement of prompt charm meson production cross-sections in $p\bar{p}$ collisions at $\sqrt{s} = 1.96$ TeV*, Phys. Rev. Lett. **91** (2003) 241804, arXiv:hep-ex/0307080.

[16] ALICE collaboration, B. Abelev *et al.*, *Measurement of charm production at central rapidity in proton-proton collisions at $\sqrt{s} = 2.76$ TeV*, JHEP **07** (2012) 191, arXiv:1205.4007.

[17] ALICE collaboration, B. Abelev *et al.*, *D_s^+ meson production at central rapidity in proton–proton collisions at $\sqrt{s} = 7$ TeV*, Phys. Lett. **B718** (2012) 279, arXiv:1208.1948.

[18] ALICE collaboration, B. Abelev *et al.*, *Measurement of charm production at central rapidity in proton-proton collisions at $\sqrt{s} = 7$ TeV*, JHEP **01** (2012) 128, arXiv:1111.1553.

[19] ALICE collaboration, J. Adam *et al.*, *D-meson production in p-Pb collisions at $\sqrt{s_{\rm NN}} = 5.02$ TeV and in pp collisions at $\sqrt{s} = 7$ TeV*, arXiv:1605.07569.

[20] ATLAS, G. Aad *et al.*, *Measurement of $D^{*\pm}$, $D^{\pm}$ and $D_s^{\pm}$ meson production cross sections in pp collisions at $\sqrt{s} = 7$ TeV with the ATLAS detector*, Nucl. Phys. **B907** (2016) 717, arXiv:1512.02913.

[21] LHCb collaboration, R. Aaij *et al.*, *Prompt charm production in pp collisions at $\sqrt{s} = 7$ TeV*, Nucl. Phys. **B871** (2013) 1, arXiv:1302.2864.

[22] LHCb collaboration, R. Aaij *et al.*, *Measurements of prompt charm production cross-sections in pp collisions at $\sqrt{s} = 13$ TeV*, JHEP **03** (2016) 159, Erratum ibid. **09** (2016) 013, arXiv:1510.01707, 2nd Erratum submitted.

[23] LHCb collaboration, A. A. Alves Jr. *et al.*, *The LHCb detector at the LHC*, JINST **3** (2008) S08005.

[24] LHCb collaboration, R. Aaij *et al.*, *LHCb detector performance*, Int. J. Mod. Phys. **A30** (2015) 1530022, arXiv:1412.6352.

[25] G. Dujany and B. Storaci, *Real-time alignment and calibration of the LHCb Detector in Run II*, J. Phys. Conf. Ser. **664** (2015) 082010.

[26] R. Aaij *et al.*, *The LHCb trigger and its performance in 2011*, JINST **8** (2013) P04022, arXiv:1211.3055.

[27] R. Aaij *et al.*, *Tesla: An application for real-time data analysis in High Energy Physics*, arXiv:1604.05596.

[28] T. Sjöstrand, S. Mrenna, and P. Skands, *PYTHIA 6.4 physics and manual*, JHEP **05** (2006) 026, arXiv:hep-ph/0603175.

[29] T. Sjöstrand, S. Mrenna, and P. Skands, *A brief introduction to PYTHIA 8.1*, Comput. Phys. Commun. **178** (2008) 852, arXiv:0710.3820.

[30] I. Belyaev *et al.*, *Handling of the generation of primary events in Gauss, the LHCb simulation framework*, J. Phys. Conf. Ser. **331** (2011) 032047.

[31] D. J. Lange, *The EvtGen particle decay simulation package*, Nucl. Instrum. Meth. **A462** (2001) 152.

[32] P. Golonka and Z. Was, *PHOTOS Monte Carlo: A precision tool for QED corrections in Z and W decays*, Eur. Phys. J. **C45** (2006) 97, arXiv:hep-ph/0506026.

[33] Geant4 collaboration, J. Allison *et al.*, *Geant4 developments and applications*, IEEE Trans. Nucl. Sci. **53** (2006) 270; Geant4 collaboration, S. Agostinelli *et al.*, *Geant4: A simulation toolkit*, Nucl. Instrum. Meth. **A506** (2003) 250.

[34] M. Clemencic *et al.*, *The LHCb simulation application, Gauss: Design, evolution and experience*, J. Phys. Conf. Ser. **331** (2011) 032023.

[35] M. Pivk and F. R. Le Diberder, *sPlot: A statistical tool to unfold data distributions*, Nucl. Instrum. Meth. **A555** (2005) 356, arXiv:physics/0402083.

[36] LHCb collaboration, R. Aaij *et al.*, *Measurement of the track reconstruction efficiency at LHCb*, JINST **10** (2015) P02007, arXiv:1408.1251.

[37] Particle Data Group, K. A. Olive *et al.*, *Review of particle physics*, Chin. Phys. **C38** (2014) 090001, and 2015 update.

[38] LHCb collaboration, R. Aaij *et al.*, *Precision luminosity measurements at LHCb*, JINST **9** (2014) P12005, arXiv:1410.0149.

[39] Particle Data Group, K. A. Olive *et al.*, *Review of particle physics*, Chin. Phys. **C38** (2014) 090001.

[40] CLEO collaboration, J. P. Alexander *et al.*, *Absolute measurement of hadronic branching fractions of the $D^+_{(s)}$ meson*, Phys. Rev. Lett. **100** (2008) 161804, arXiv:0801.0680.

[41] CLEO collaboration, M. Artuso *et al.*, *Charm meson spectra in e^+e^- annihilation at 10.5 GeV center of mass energy*, Phys. Rev. **D70** (2004) 112001, arXiv:hep-ex/0402040.

[42] Belle collaboration, R. Seuster *et al.*, *Charm hadrons from fragmentation and B decays in e^+e^- annihilation at $\sqrt{s} = 10.6\,GeV$*, Phys. Rev. **D73** (2006) 032002, arXiv:hep-ex/0506068.

[43] BaBar collaboration, B. Aubert *et al.*, *Measurement of D_s^+ and D_s^{*+} production in B meson decays and from continuum e^+e^- annihilation at $\sqrt{s} = 10.6\,GeV$*, Phys. Rev. **D65** (2002) 091104, arXiv:hep-ex/0201041.

[44] Particle Data Group, C. Amsler *et al.*, *Fragmentation functions in e^+e^- annihilation and lepton-nucleon DIS,* in *Review of particle physics*, Phys. Lett. **B667** (2008) 1.

[45] L. Lyons, D. Gibaut, and P. Clifford, *How to combine correlated estimates of a single physical quantity*, Nucl. Instrum. Meth. **A270** (1988) 110.

[46] NNPDF collaboration, R. D. Ball *et al.*, *Parton distributions for the LHC Run II*, JHEP **04** (2015) 040, arXiv:1410.8849.

[47] S. Alioli, P. Nason, C. Oleari, and E. Re, *A general framework for implementing NLO calculations in shower Monte Carlo programs: The POWHEG BOX*, JHEP **06** (2010) 043, arXiv:1002.2581.

[48] T. Sjöstrand *et al.*, *An introduction to PYTHIA 8.2*, Comput. Phys. Commun. **191** (2015) 159, arXiv:1410.3012.

[49] H.-L. Lai *et al.*, *New parton distributions for collider physics*, Phys. Rev. **D82** (2010) 074024, arXiv:1007.2241.

[50] B. A. Kniehl and G. Kramer, *Charmed-hadron fragmentation functions from CERN LEP1 revisited*, Phys. Rev. **D74** (2006) 037502, arXiv:hep-ph/0607306.

LHCb collaboration

R. Aaij[40], B. Adeva[39], M. Adinolfi[48], Z. Ajaltouni[5], S. Akar[6], J. Albrecht[10], F. Alessio[40], M. Alexander[53], S. Ali[43], G. Alkhazov[31], P. Alvarez Cartelle[55], A.A. Alves Jr[59], S. Amato[2], S. Amerio[23], Y. Amhis[7], L. An[41], L. Anderlini[18], G. Andreassi[41], M. Andreotti[17,g], J.E. Andrews[60], R.B. Appleby[56], F. Archilli[43], P. d'Argent[12], J. Arnau Romeu[6], A. Artamonov[37], M. Artuso[61], E. Aslanides[6], G. Auriemma[26], M. Baalouch[5], I. Babuschkin[56], S. Bachmann[12], J.J. Back[50], A. Badalov[38], C. Baesso[62], S. Baker[55], W. Baldini[17], R.J. Barlow[56], C. Barschel[40], S. Barsuk[7], W. Barter[40], M. Baszczyk[27], V. Batozskaya[29], B. Batsukh[61], V. Battista[41], A. Bay[41], L. Beaucourt[4], J. Beddow[53], F. Bedeschi[24], I. Bediaga[1], L.J. Bel[43], V. Bellee[41], N. Belloli[21,i], K. Belous[37], I. Belyaev[32], E. Ben-Haim[8], G. Bencivenni[19], S. Benson[43], J. Benton[48], A. Berezhnoy[33], R. Bernet[42], A. Bertolin[23], C. Betancourt[42], F. Betti[15], M.-O. Bettler[40], M. van Beuzekom[43], Ia. Bezshyiko[42], S. Bifani[47], P. Billoir[8], T. Bird[56], A. Birnkraut[10], A. Bitadze[56], A. Bizzeti[18,u], T. Blake[50], F. Blanc[41], J. Blouw[11,†], S. Blusk[61], V. Bocci[26], T. Boettcher[58], A. Bondar[36,w], N. Bondar[31,40], W. Bonivento[16], I. Bordyuzhin[32], A. Borgheresi[21,i], S. Borghi[56], M. Borisyak[35], M. Borsato[39], F. Bossu[7], M. Boubdir[9], T.J.V. Bowcock[54], E. Bowen[42], C. Bozzi[17,40], S. Braun[12], M. Britsch[12], T. Britton[61], J. Brodzicka[56], E. Buchanan[48], C. Burr[56], A. Bursche[2], J. Buytaert[40], S. Cadeddu[16], R. Calabrese[17,g], M. Calvi[21,i], M. Calvo Gomez[38,m], A. Camboni[38], P. Campana[19], D.H. Campora Perez[40], L. Capriotti[56], A. Carbone[15,e], G. Carboni[25,j], R. Cardinale[20,h], A. Cardini[16], P. Carniti[21,i], L. Carson[52], K. Carvalho Akiba[2], G. Casse[54], L. Cassina[21,i], L. Castillo Garcia[41], M. Cattaneo[40], Ch. Cauet[10], G. Cavallero[20], R. Cenci[24,t], D. Chamont[7], M. Charles[8], Ph. Charpentier[40], G. Chatzikonstantinidis[47], M. Chefdeville[4], S. Chen[56], S.-F. Cheung[57], V. Chobanova[39], M. Chrzaszcz[42,27], X. Cid Vidal[39], G. Ciezarek[43], P.E.L. Clarke[52], M. Clemencic[40], H.V. Cliff[49], J. Closier[40], V. Coco[59], J. Cogan[6], E. Cogneras[5], V. Cogoni[16,40,f], L. Cojocariu[30], G. Collazuol[23,o], P. Collins[40], A. Comerma-Montells[12], A. Contu[40], A. Cook[48], G. Coombs[40], S. Coquereau[38], G. Corti[40], M. Corvo[17,g], C.M. Costa Sobral[50], B. Couturier[40], G.A. Cowan[52], D.C. Craik[52], A. Crocombe[50], M. Cruz Torres[62], S. Cunliffe[55], R. Currie[55], C. D'Ambrosio[40], F. Da Cunha Marinho[2], E. Dall'Occo[43], J. Dalseno[48], P.N.Y. David[43], A. Davis[59], O. De Aguiar Francisco[2], K. De Bruyn[6], S. De Capua[56], M. De Cian[12], J.M. De Miranda[1], L. De Paula[2], M. De Serio[14,d], P. De Simone[19], C.-T. Dean[53], D. Decamp[4], M. Deckenhoff[10], L. Del Buono[8], M. Demmer[10], A. Dendek[28], D. Derkach[35], O. Deschamps[5], F. Dettori[40], B. Dey[22], A. Di Canto[40], H. Dijkstra[40], F. Dordei[40], M. Dorigo[41], A. Dosil Suárez[39], A. Dovbnya[45], K. Dreimanis[54], L. Dufour[43], G. Dujany[56], K. Dungs[40], P. Durante[40], R. Dzhelyadin[37], A. Dziurda[40], A. Dzyuba[31], N. Déléage[4], S. Easo[51], M. Ebert[52], U. Egede[55], V. Egorychev[32], S. Eidelman[36,w], S. Eisenhardt[52], U. Eitschberger[10], R. Ekelhof[10], L. Eklund[53], S. Ely[61], S. Esen[12], H.M. Evans[49], T. Evans[57], A. Falabella[15], N. Farley[47], S. Farry[54], R. Fay[54], D. Fazzini[21,i], D. Ferguson[52], A. Fernandez Prieto[39], F. Ferrari[15,40], F. Ferreira Rodrigues[2], M. Ferro-Luzzi[40], S. Filippov[34], R.A. Fini[14], M. Fiore[17,g], M. Fiorini[17,g], M. Firlej[28], C. Fitzpatrick[41], T. Fiutowski[28], F. Fleuret[7,b], K. Fohl[40], M. Fontana[16,40], F. Fontanelli[20,h], D.C. Forshaw[61], R. Forty[40], V. Franco Lima[54], M. Frank[40], C. Frei[40], J. Fu[22,q], E. Furfaro[25,j], C. Färber[40], A. Gallas Torreira[39], D. Galli[15,e], S. Gallorini[23], S. Gambetta[52], M. Gandelman[2], P. Gandini[57], Y. Gao[3], L.M. Garcia Martin[68], J. García Pardiñas[39], J. Garra Tico[49], L. Garrido[38], P.J. Garsed[49], D. Gascon[38], C. Gaspar[40], L. Gavardi[10], G. Gazzoni[5], D. Gerick[12], E. Gersabeck[12], M. Gersabeck[56], T. Gershon[50], Ph. Ghez[4], S. Gianì[41], V. Gibson[49], O.G. Girard[41], L. Giubega[30], K. Gizdov[52], V.V. Gligorov[8], D. Golubkov[32], A. Golutvin[55,40], A. Gomes[1,a], I.V. Gorelov[33], C. Gotti[21,i], M. Grabalosa Gándara[5], R. Graciani Diaz[38], L.A. Granado Cardoso[40], E. Graugés[38], E. Graverini[42], G. Graziani[18], A. Grecu[30], P. Griffith[47], L. Grillo[21,40,i], B.R. Gruberg Cazon[57], O. Grünberg[66], E. Gushchin[34], Yu. Guz[37], T. Gys[40],

C. Göbel[62], T. Hadavizadeh[57], C. Hadjivasiliou[5], G. Haefeli[41], C. Haen[40], S.C. Haines[49], S. Hall[55], B. Hamilton[60], X. Han[12], S. Hansmann-Menzemer[12], N. Harnew[57], S.T. Harnew[48], J. Harrison[56], M. Hatch[40], J. He[63], T. Head[41], A. Heister[9], K. Hennessy[54], P. Henrard[5], L. Henry[8], J.A. Hernando Morata[39], E. van Herwijnen[40], M. Heß[66], A. Hicheur[2], D. Hill[57], C. Hombach[56], H. Hopchev[41], W. Hulsbergen[43], T. Humair[55], M. Hushchyn[35], N. Hussain[57], D. Hutchcroft[54], M. Idzik[28], P. Ilten[58], R. Jacobsson[40], A. Jaeger[12], J. Jalocha[57], E. Jans[43], A. Jawahery[60], F. Jiang[3], M. John[57], D. Johnson[40], C.R. Jones[49], C. Joram[40], B. Jost[40], N. Jurik[61], S. Kandybei[45], W. Kanso[6], M. Karacson[40], J.M. Kariuki[48], S. Karodia[53], M. Kecke[12], M. Kelsey[61], I.R. Kenyon[47], M. Kenzie[49], T. Ketel[44], E. Khairullin[35], B. Khanji[12], C. Khurewathanakul[41], T. Kirn[9], S. Klaver[56], K. Klimaszewski[29], S. Koliiev[46], M. Kolpin[12], I. Komarov[41], R.F. Koopman[44], P. Koppenburg[43], A. Kosmyntseva[32], A. Kozachuk[33], M. Kozeiha[5], L. Kravchuk[34], K. Kreplin[12], M. Kreps[50], P. Krokovny[36,w], F. Kruse[10], W. Krzemien[29], W. Kucewicz[27,l], M. Kucharczyk[27], V. Kudryavtsev[36,w], A.K. Kuonen[41], K. Kurek[29], T. Kvaratskheliya[32,40], D. Lacarrere[40], G. Lafferty[56], A. Lai[16], G. Lanfranchi[19], C. Langenbruch[9], T. Latham[50], C. Lazzeroni[47], R. Le Gac[6], J. van Leerdam[43], J.-P. Lees[4], A. Leflat[33,40], J. Lefrançois[7], R. Lefèvre[5], F. Lemaitre[40], E. Lemos Cid[39], O. Leroy[6], T. Lesiak[27], B. Leverington[12], Y. Li[7], T. Likhomanenko[35,67], R. Lindner[40], C. Linn[40], F. Lionetto[42], B. Liu[16], X. Liu[3], D. Loh[50], I. Longstaff[53], J.H. Lopes[2], D. Lucchesi[23,o], M. Lucio Martinez[39], H. Luo[52], A. Lupato[23], E. Luppi[17,g], O. Lupton[57], A. Lusiani[24], X. Lyu[63], F. Machefert[7], F. Maciuc[30], O. Maev[31], K. Maguire[56], S. Malde[57], A. Malinin[67], T. Maltsev[36], G. Manca[7], G. Mancinelli[6], P. Manning[61], J. Maratas[5,v], J.F. Marchand[4], U. Marconi[15], C. Marin Benito[38], P. Marino[24,t], J. Marks[12], G. Martellotti[26], M. Martin[6], M. Martinelli[41], D. Martinez Santos[39], F. Martinez Vidal[68], D. Martins Tostes[2], L.M. Massacrier[7], A. Massafferri[1], R. Matev[40], A. Mathad[50], Z. Mathe[40], C. Matteuzzi[21], A. Mauri[42], B. Maurin[41], A. Mazurov[47], M. McCann[55], J. McCarthy[47], A. McNab[56], R. McNulty[13], B. Meadows[59], F. Meier[10], M. Meissner[12], D. Melnychuk[29], M. Merk[43], A. Merli[22,q], E. Michielin[23], D.A. Milanes[65], M.-N. Minard[4], D.S. Mitzel[12], A. Mogini[8], J. Molina Rodriguez[1], I.A. Monroy[65], S. Monteil[5], M. Morandin[23], P. Morawski[28], A. Mordà[6], M.J. Morello[24,t], J. Moron[28], A.B. Morris[52], R. Mountain[61], F. Muheim[52], M. Mulder[43], M. Mussini[15], D. Müller[56], J. Müller[10], K. Müller[42], V. Müller[10], P. Naik[48], T. Nakada[41], R. Nandakumar[51], A. Nandi[57], I. Nasteva[2], M. Needham[52], N. Neri[22], S. Neubert[12], N. Neufeld[40], M. Neuner[12], A.D. Nguyen[41], T.D. Nguyen[41], C. Nguyen-Mau[41,n], S. Nieswand[9], R. Niet[10], N. Nikitin[33], T. Nikodem[12], A. Novoselov[37], D.P. O'Hanlon[50], A. Oblakowska-Mucha[28], V. Obraztsov[37], S. Ogilvy[19], R. Oldeman[49], C.J.G. Onderwater[69], J.M. Otalora Goicochea[2], A. Otto[40], P. Owen[42], A. Oyanguren[68,40], P.R. Pais[41], A. Palano[14,d], F. Palombo[22,q], M. Palutan[19], J. Panman[40], A. Papanestis[51], M. Pappagallo[14,d], L.L. Pappalardo[17,g], W. Parker[60], C. Parkes[56], G. Passaleva[18], A. Pastore[14,d], G.D. Patel[54], M. Patel[55], C. Patrignani[15,e], A. Pearce[56,51], A. Pellegrino[43], G. Penso[26], M. Pepe Altarelli[40], S. Perazzini[40], P. Perret[5], L. Pescatore[47], K. Petridis[48], A. Petrolini[20,h], A. Petrov[67], M. Petruzzo[22,q], E. Picatoste Olloqui[38], B. Pietrzyk[4], M. Pikies[27], D. Pinci[26], A. Pistone[20], A. Piucci[12], S. Playfer[52], M. Plo Casasus[39], T. Poikela[40], F. Polci[8], A. Poluektov[50,36], I. Polyakov[61], E. Polycarpo[2], G.J. Pomery[48], A. Popov[37], D. Popov[11,40], B. Popovici[30], S. Poslavskii[37], C. Potterat[2], E. Price[48], J.D. Price[54], J. Prisciandaro[39], A. Pritchard[54], C. Prouve[48], V. Pugatch[46], A. Puig Navarro[41], G. Punzi[24,p], W. Qian[57], R. Quagliani[7,48], B. Rachwal[27], J.H. Rademacker[48], M. Rama[24], M. Ramos Pernas[39], M.S. Rangel[2], I. Raniuk[45], F. Ratnikov[35], G. Raven[44], F. Redi[55], S. Reichert[10], A.C. dos Reis[1], C. Remon Alepuz[68], V. Renaudin[7], S. Ricciardi[51], S. Richards[48], M. Rihl[40], K. Rinnert[54], V. Rives Molina[38], P. Robbe[7,40], A.B. Rodrigues[1], E. Rodrigues[59], J.A. Rodriguez Lopez[65], P. Rodriguez Perez[56,†], A. Rogozhnikov[35], S. Roiser[40], A. Rollings[57], V. Romanovskiy[37], A. Romero Vidal[39], J.W. Ronayne[13], M. Rotondo[19], M.S. Rudolph[61], T. Ruf[40], P. Ruiz Valls[68], J.J. Saborido Silva[39], E. Sadykhov[32], N. Sagidova[31], B. Saitta[16,f],

V. Salustino Guimaraes[2], C. Sanchez Mayordomo[68], B. Sanmartin Sedes[39], R. Santacesaria[26], C. Santamarina Rios[39], M. Santimaria[19], E. Santovetti[25,j], A. Sarti[19,k], C. Satriano[26,s], A. Satta[25], D.M. Saunders[48], D. Savrina[32,33], S. Schael[9], M. Schellenberg[10], M. Schiller[40], H. Schindler[40], M. Schlupp[10], M. Schmelling[11], T. Schmelzer[10], B. Schmidt[40], O. Schneider[41], A. Schopper[40], K. Schubert[10], M. Schubiger[41], M.-H. Schune[7], R. Schwemmer[40], B. Sciascia[19], A. Sciubba[26,k], A. Semennikov[32], A. Sergi[47], N. Serra[42], J. Serrano[6], L. Sestini[23], P. Seyfert[21], M. Shapkin[37], I. Shapoval[45], Y. Shcheglov[31], T. Shears[54], L. Shekhtman[36,w], V. Shevchenko[67], B.G. Siddi[17,40], R. Silva Coutinho[42], L. Silva de Oliveira[2], G. Simi[23,o], S. Simone[14,d], M. Sirendi[49], N. Skidmore[48], T. Skwarnicki[61], E. Smith[55], I.T. Smith[52], J. Smith[49], M. Smith[55], H. Snoek[43], M.D. Sokoloff[59], F.J.P. Soler[53], B. Souza De Paula[2], B. Spaan[10], P. Spradlin[53], S. Sridharan[40], F. Stagni[40], M. Stahl[12], S. Stahl[40], P. Stefko[41], S. Stefkova[55], O. Steinkamp[42], S. Stemmle[12], O. Stenyakin[37], S. Stevenson[57], S. Stoica[30], S. Stone[61], B. Storaci[42], S. Stracka[24,p], M. Straticiuc[30], U. Straumann[42], L. Sun[59], W. Sutcliffe[55], K. Swientek[28], V. Syropoulos[44], M. Szczekowski[29], T. Szumlak[28], S. T'Jampens[4], A. Tayduganov[6], T. Tekampe[10], G. Tellarini[17,g], F. Teubert[40], E. Thomas[40], J. van Tilburg[43], M.J. Tilley[55], V. Tisserand[4], M. Tobin[41], S. Tolk[49], L. Tomassetti[17,g], D. Tonelli[40], S. Topp-Joergensen[57], F. Toriello[61], E. Tournefier[4], S. Tourneur[41], K. Trabelsi[41], M. Traill[53], M.T. Tran[41], M. Tresch[42], A. Trisovic[40], A. Tsaregorodtsev[6], P. Tsopelas[43], A. Tully[49], N. Tuning[43], A. Ukleja[29], A. Ustyuzhanin[35], U. Uwer[12], C. Vacca[16,f], V. Vagnoni[15,40], A. Valassi[40], S. Valat[40], G. Valenti[15], A. Vallier[7], R. Vazquez Gomez[19], P. Vazquez Regueiro[39], S. Vecchi[17], M. van Veghel[43], J.J. Velthuis[48], M. Veltri[18,r], G. Veneziano[57], A. Venkateswaran[61], M. Vernet[5], M. Vesterinen[12], B. Viaud[7], D. Vieira[1], M. Vieites Diaz[39], H. Viemann[66], X. Vilasis-Cardona[38,m], M. Vitti[49], V. Volkov[33], A. Vollhardt[42], B. Voneki[40], A. Vorobyev[31], V. Vorobyev[36,w], C. Voß[66], J.A. de Vries[43], C. Vázquez Sierra[39], R. Waldi[66], C. Wallace[50], R. Wallace[13], J. Walsh[24], J. Wang[61], D.R. Ward[49], H.M. Wark[54], N.K. Watson[47], D. Websdale[55], A. Weiden[42], M. Whitehead[40], J. Wicht[50], G. Wilkinson[57,40], M. Wilkinson[61], M. Williams[40], M.P. Williams[47], M. Williams[58], T. Williams[47], F.F. Wilson[51], J. Wimberley[60], J. Wishahi[10], W. Wislicki[29], M. Witek[27], G. Wormser[7], S.A. Wotton[49], K. Wraight[53], K. Wyllie[40], Y. Xie[64], Z. Xing[61], Z. Xu[41], Z. Yang[3], Y. Yao[61], H. Yin[64], J. Yu[64], X. Yuan[36,w], O. Yushchenko[37], K.A. Zarebski[47], M. Zavertyaev[11,c], L. Zhang[3], Y. Zhang[7], Y. Zhang[63], A. Zhelezov[12], Y. Zheng[63], A. Zhokhov[32], X. Zhu[3], V. Zhukov[9], S. Zucchelli[15].

[1] *Centro Brasileiro de Pesquisas Físicas (CBPF), Rio de Janeiro, Brazil*
[2] *Universidade Federal do Rio de Janeiro (UFRJ), Rio de Janeiro, Brazil*
[3] *Center for High Energy Physics, Tsinghua University, Beijing, China*
[4] *LAPP, Université Savoie Mont-Blanc, CNRS/IN2P3, Annecy-Le-Vieux, France*
[5] *Clermont Université, Université Blaise Pascal, CNRS/IN2P3, LPC, Clermont-Ferrand, France*
[6] *CPPM, Aix-Marseille Université, CNRS/IN2P3, Marseille, France*
[7] *LAL, Université Paris-Sud, CNRS/IN2P3, Orsay, France*
[8] *LPNHE, Université Pierre et Marie Curie, Université Paris Diderot, CNRS/IN2P3, Paris, France*
[9] *I. Physikalisches Institut, RWTH Aachen University, Aachen, Germany*
[10] *Fakultät Physik, Technische Universität Dortmund, Dortmund, Germany*
[11] *Max-Planck-Institut für Kernphysik (MPIK), Heidelberg, Germany*
[12] *Physikalisches Institut, Ruprecht-Karls-Universität Heidelberg, Heidelberg, Germany*
[13] *School of Physics, University College Dublin, Dublin, Ireland*
[14] *Sezione INFN di Bari, Bari, Italy*
[15] *Sezione INFN di Bologna, Bologna, Italy*
[16] *Sezione INFN di Cagliari, Cagliari, Italy*
[17] *Sezione INFN di Ferrara, Ferrara, Italy*
[18] *Sezione INFN di Firenze, Firenze, Italy*
[19] *Laboratori Nazionali dell'INFN di Frascati, Frascati, Italy*
[20] *Sezione INFN di Genova, Genova, Italy*
[21] *Sezione INFN di Milano Bicocca, Milano, Italy*

[22] *Sezione INFN di Milano, Milano, Italy*
[23] *Sezione INFN di Padova, Padova, Italy*
[24] *Sezione INFN di Pisa, Pisa, Italy*
[25] *Sezione INFN di Roma Tor Vergata, Roma, Italy*
[26] *Sezione INFN di Roma La Sapienza, Roma, Italy*
[27] *Henryk Niewodniczanski Institute of Nuclear Physics Polish Academy of Sciences, Kraków, Poland*
[28] *AGH - University of Science and Technology, Faculty of Physics and Applied Computer Science, Kraków, Poland*
[29] *National Center for Nuclear Research (NCBJ), Warsaw, Poland*
[30] *Horia Hulubei National Institute of Physics and Nuclear Engineering, Bucharest-Magurele, Romania*
[31] *Petersburg Nuclear Physics Institute (PNPI), Gatchina, Russia*
[32] *Institute of Theoretical and Experimental Physics (ITEP), Moscow, Russia*
[33] *Institute of Nuclear Physics, Moscow State University (SINP MSU), Moscow, Russia*
[34] *Institute for Nuclear Research of the Russian Academy of Sciences (INR RAN), Moscow, Russia*
[35] *Yandex School of Data Analysis, Moscow, Russia*
[36] *Budker Institute of Nuclear Physics (SB RAS), Novosibirsk, Russia, Novosibirsk, Russia*
[37] *Institute for High Energy Physics (IHEP), Protvino, Russia*
[38] *ICCUB, Universitat de Barcelona, Barcelona, Spain*
[39] *Universidad de Santiago de Compostela, Santiago de Compostela, Spain*
[40] *European Organization for Nuclear Research (CERN), Geneva, Switzerland*
[41] *Ecole Polytechnique Fédérale de Lausanne (EPFL), Lausanne, Switzerland*
[42] *Physik-Institut, Universität Zürich, Zürich, Switzerland*
[43] *Nikhef National Institute for Subatomic Physics, Amsterdam, The Netherlands*
[44] *Nikhef National Institute for Subatomic Physics and VU University Amsterdam, Amsterdam, The Netherlands*
[45] *NSC Kharkiv Institute of Physics and Technology (NSC KIPT), Kharkiv, Ukraine*
[46] *Institute for Nuclear Research of the National Academy of Sciences (KINR), Kyiv, Ukraine*
[47] *University of Birmingham, Birmingham, United Kingdom*
[48] *H.H. Wills Physics Laboratory, University of Bristol, Bristol, United Kingdom*
[49] *Cavendish Laboratory, University of Cambridge, Cambridge, United Kingdom*
[50] *Department of Physics, University of Warwick, Coventry, United Kingdom*
[51] *STFC Rutherford Appleton Laboratory, Didcot, United Kingdom*
[52] *School of Physics and Astronomy, University of Edinburgh, Edinburgh, United Kingdom*
[53] *School of Physics and Astronomy, University of Glasgow, Glasgow, United Kingdom*
[54] *Oliver Lodge Laboratory, University of Liverpool, Liverpool, United Kingdom*
[55] *Imperial College London, London, United Kingdom*
[56] *School of Physics and Astronomy, University of Manchester, Manchester, United Kingdom*
[57] *Department of Physics, University of Oxford, Oxford, United Kingdom*
[58] *Massachusetts Institute of Technology, Cambridge, MA, United States*
[59] *University of Cincinnati, Cincinnati, OH, United States*
[60] *University of Maryland, College Park, MD, United States*
[61] *Syracuse University, Syracuse, NY, United States*
[62] *Pontifícia Universidade Católica do Rio de Janeiro (PUC-Rio), Rio de Janeiro, Brazil, associated to* [2]
[63] *University of Chinese Academy of Sciences, Beijing, China, associated to* [3]
[64] *Institute of Particle Physics, Central China Normal University, Wuhan, Hubei, China, associated to* [3]
[65] *Departamento de Fisica , Universidad Nacional de Colombia, Bogota, Colombia, associated to* [8]
[66] *Institut für Physik, Universität Rostock, Rostock, Germany, associated to* [12]
[67] *National Research Centre Kurchatov Institute, Moscow, Russia, associated to* [32]
[68] *Instituto de Fisica Corpuscular (IFIC), Universitat de Valencia-CSIC, Valencia, Spain, associated to* [38]
[69] *Van Swinderen Institute, University of Groningen, Groningen, The Netherlands, associated to* [43]

[a] *Universidade Federal do Triângulo Mineiro (UFTM), Uberaba-MG, Brazil*
[b] *Laboratoire Leprince-Ringuet, Palaiseau, France*
[c] *P.N. Lebedev Physical Institute, Russian Academy of Science (LPI RAS), Moscow, Russia*
[d] *Università di Bari, Bari, Italy*
[e] *Università di Bologna, Bologna, Italy*
[f] *Università di Cagliari, Cagliari, Italy*

[g] *Università di Ferrara, Ferrara, Italy*
[h] *Università di Genova, Genova, Italy*
[i] *Università di Milano Bicocca, Milano, Italy*
[j] *Università di Roma Tor Vergata, Roma, Italy*
[k] *Università di Roma La Sapienza, Roma, Italy*
[l] *AGH - University of Science and Technology, Faculty of Computer Science, Electronics and Telecommunications, Kraków, Poland*
[m] *LIFAELS, La Salle, Universitat Ramon Llull, Barcelona, Spain*
[n] *Hanoi University of Science, Hanoi, Viet Nam*
[o] *Università di Padova, Padova, Italy*
[p] *Università di Pisa, Pisa, Italy*
[q] *Università degli Studi di Milano, Milano, Italy*
[r] *Università di Urbino, Urbino, Italy*
[s] *Università della Basilicata, Potenza, Italy*
[t] *Scuola Normale Superiore, Pisa, Italy*
[u] *Università di Modena e Reggio Emilia, Modena, Italy*
[v] *Iligan Institute of Technology (IIT), Iligan, Philippines*
[w] *Novosibirsk State University, Novosibirsk, Russia*

[†] *Deceased*